Protein kinase C gamma interneurons in the rat medullary dorsal horn: distribution and synaptic inputs of these neurons, and subcellular localization of the enzyme

Cédric Peirs, Sudarshan Patil, Rabia Bouali-Benazzouz, Alain Artola, Marc Landry, Radhouane Dallel

Protein kinase C gamma interneurons in the rat medullary dorsal horn: distribution and synaptic inputs of these neurons, and subcellular localization of the enzyme

Cédric Peirs[1], Sudarshan Patil[1], Rabia Bouali-Benazzouz[2], Alain Artola[1], Marc Landry[2], Radhouane Dallel[1]

[1]Inserm/UdA U1107, Neuro-Dol: Trigeminal Pain and Migraine, Université d'Auvergne, Faculté de Chirurgie Dentaire, 11 Boulevard Charles de Gaulle, Clermont-Ferrand, 63000, France. [2]IINS, CNRS UMR 5297, Bordeaux Segalen University, Université Bordeaux 2, 146 rue Leo-Saignat, Bordeaux, 33077, France

Present address for Dr. Sudarshan Patil is Neuroscience research group, Institute of Biomedicine, University of Bergen, Jonas Lies vei 91, N-5009, Bergen, Norway.

Running head: PKCγ interneurons in rat MDH

Associate editor: Gert Holstege, University of Groningen: Brainstem and Spinal Cord Sensorimotor Systems

Corresponding author : Pr. Radhouane DALLEL

Inserm/UdA U1107, Neuro-Dol: Trigeminal Pain and Migraine, Faculté de Chirurgie Dentaire, 11 Boulevard Charles de Gaulle, Clermont-Ferrand, 63000, France.

Tel: +33-4-7317-7313, Fax: +33-4-7317-7306, E-mail : radhouane.dallel@udamail.fr

Grant Information: Institut National de la Santé et de la Recherche Médicale (INSERM), Centre National de la Recherche Scientifique (CNRS), Ministère de l'Enseignement Supérieur et de la Recherche, Fondation des Gueules Cassées, Université d'Auvergne-Clermont1 (France) and Région Auvergne.

ABSTRACT

The γ isoform of protein kinase C (PKCγ), which is concentrated in interneurons in the inner part of lamina II (II_i) of the dorsal horn, has been implicated in the expression of tactile allodynia. Lamina II_i PKCγ interneurons were shown to be activated by tactile inputs and to participate in local circuits through which these inputs can reach lamina I, nociceptive output neurons. That such local circuits are gated by glycinergic inhibition and that A- and C-fibers low threshold mechanoreceptors (LTMRs) terminate in lamina II_i raise the general issue of synaptic inputs to lamina II_i PKCγ interneurons. Combining light and electron microscopic immunochemistry in the rat spinal trigeminal nucleus, we show that PKCγ-immunoreactivity is mostly restricted to interneurons in lamina II_i of the medullary dorsal horn, where they constitute 1/3 of total neurons. The majority of synapses on PKCγ-immunoreactive interneurons are asymmetric (likely excitatory). PKCγ-immunoreactive interneurons appear to receive exclusively myelinated primary afferents in type II synaptic glomeruli. Neither large dense core vesicle terminals nor type I synaptic glomeruli, assumed to be the endings of unmyelinated nociceptive terminals, were found on these interneurons. Moreover, there is no vesicular glutamate transporter 3-immunoreactive boutons, specific of C-LTMRs, on PKCγ-immunoreactive interneurons. PKCγ-immunoreactive interneurons contain $GABA_A$ergic and glycinergic receptors. At subcellular level, PKCγ-immunoreactivity is mostly concentrated on plasma membranes, close to, but not within, postsynaptic densities. That only myelinated primary afferents were found to contact PKCγ-immunoreactive interneurons suggests that myelinated, but not unmyelinated, LTMRs play a critical role in the expression of mechanical allodynia.

KEY WORDS

Medullary dorsal horn (MDH), protein kinase C gamma (PKCγ), C-low threshold mechanoreceptor (C-LTMR), vesicular glutamate transporter 3 (VGLUT3), γ-aminobutyric acid type A receptor ($GABA_A$), glycine receptor, electron microscopy, confocal microscopy

INTRODUCTION

Pain is initiated by peripheral tissue damage and inflammation (inflammatory pain) or lesions to the nervous system (neuropathic pain). It is characterized by persistent pain hypersensitivity, including spontaneous pain (pain experienced in the absence of any obvious peripheral stimulus), hyperalgesia (exacerbated response to noxious stimuli) and allodynia (pain in response to normally innocuous stimuli).

It is now well established that the development and maintenance of persistent pain hypersensitivity involves, at least in part, changes in the processing of sensory information within the dorsal horn (DH). Primary afferents terminate in DH with a distribution pattern that is determined by sensory modality: fine primary afferents, either lightly myelinated Aδ- or unmyelinated C-fibers, including most nociceptors, innervate the more superficial laminae, I and outer II (II_o), whereas touch-sensing, lightly myelinated D-hair Aδ-fibers and heavily myelinated Aβ-fibers terminate in lamina inner II (II_i)-III and II_i-V, respectively (Li et al., 2011; for review see: Basbaum et al., 2009). Under physiological conditions, informations from different modalities are kept separate. However, under conditions of disinhibition, Aβ-fiber-mediated information can reach lamina I, nociceptive output neurons by way of a polysynaptic excitatory pathway (Torsney and MacDermott, 2006; Miraucourt et al., 2007). Activation of such local circuits has been shown to be associated with mechanical allodynia, leading to a miscoding of tactile information by cells that normally only detect painful stimuli (Miraucourt et al., 2007).

The γ isoform of protein kinase C (PKCγ) appears to play an important role in the development of mechanical allodynia. Increases in PKCγ activity in spinal DH are triggered by both nerve (Miletic et al., 2000; Nakajima et al., 2011) and tissue injury (Martin et al., 1999; Cheng et al., 2008). Genetic impairment of PKCγ, by the way of targeted deletion

(Malmberg et al., 1997) or RNA interference (Zou et al., 2011) decreases specifically the behavioral allodynia that occurs days after nerve injury but has no effect on normal acute pain responses. Similarly, pharmacological impairment of PKCγ inhibits mechanical allodynia that is produced by glycine receptor antagonists (Miraucourt et al., 2007). That, in DH, PKCγ is restricted to a population of local circuit interneurons in the lamina II_i (Malmberg et al., 1997; Polgar et al., 1999) has led to the suggestion that these lamina II_i interneurons participate in local circuits underlying mechanical allodynia. However, how activation of PKCγ neurons engages the 'pain' transmission circuit, is still unclear.

In the present study, we used immunocytochemistry at the light and electron microscopy level to get insights into the neuronal function of lamina II_i PKCγ-immunoreactive interneurons in rats. We first characterized PKCγ expression in the spinal trigeminal nucleus, mainly its most caudal subnucleus or medullary dorsal horn (MDH), which has received little attention (Li et al., 2001a; Li et al., 2001b), though it is a major relay nucleus for the somatosensory information from the face and meninges. We then addressed the general issue of synaptic inputs to lamina II_i PKCγ interneurons in the MDH. C-low-threshold mechanoreceptors (C-LTMR) are a subpopulation of unmyelinated, cutaneous sensory afferents that likely process pleasant and socially relevant aspects of touch (Loken et al., 2009; Olausson et al., 2010) and mechanical allodynia after inflammation or nerve injury (Seal et al., 2009). That, on the one hand, PKCγ interneurons are specifically activated by tactile, but not noxious, inputs (Miraucourt et al., 2007; Neumann et al., 2008), and, on the other hand, in mice, C-LTMRs terminate in a very restricted DH area that precisely overlaps with the band of PKCγ-immunoreactive interneurons in lamina II_i (Seal et al., 2009; Li et al., 2011), raises the question as to whether C-LTMRs directly terminate on PKCγ-immunoreactive interneurons. Fast inhibitory synaptic transmission within the DH is mediated

by both γ-aminobutyric acid (GABA)-ergic and glycinergic transmission (for review: see Zeilhofer et al., 2012). That dorsally directed local circuits underlying mechanical allodynia appear to be unmasked by selectively glycinergic receptor antagonists (Miraucourt et al., 2007; Miraucourt et al., 2009) raises the question as to whether $GABA_A$ receptors are also present on lamina II_i PKCγ interneurons. Therefore, we examined whether both glycinergic and $GABA_A$ergic receptors are present on lamina II_i PKCγ interneurons. Finally, we examined the subcellular localization of PKCγ within lamina II_i interneurons in baseline conditions.

MATERIAL AND METHODS

Animals

Adult male Sprague–Dawley rats (250 - 275 g) were obtained from Charles River (L'Arbresle, France) and maintained in a controlled environment (light on 19.00 - 7.00, 22°C). Water and food were provided *ad libitum*. Rats were housed 3-4 per cage. All efforts were made to minimize the number of animals used. The experiments followed the ethical guidelines of the International Association for the Study of Pain and ethical guidelines of the Directive 2010/63/UE of the European Parliament and of the Council on the protection of animals used for scientific purpose.

Antibody characterization

Details of the primary antibodies used in the present study are provided in Table 1.

$GABA_A$ receptor

$GABA_A$ receptor purified monoclonal antibody BD17 (IgG1) was raised in mouse and recognizes an epitope on the extracellular domain of the β2 and β3 subunits of the $GABA_A$ receptor. The immunogen was a GABA/benzodiazepine receptor purified from bovine cortex.

This antibody reveals two proteins bands corresponding to the β3 (57kDa) and β2 (55 kDa) subunits in Western blot analysis of both rat brain and spinal cord lysates (Fig. 1). Staining is eliminated by replacing primary antibodies with nonimmune serum (Fig. 1).

Glycine receptor

Glycine receptor α purified monoclonal antibody mAb4a (IgG1) was raised in mouse and recognizes an epitope located within the amino acid residues 99-105 of the N-terminal region of the mature glycine receptor α1-subunit. The immunogen was a purified rat spinal cord glycine receptor. This antibody reveals the appropriate protein band (48 kDa) on Western blot analysis of rat spinal cord (Fig. 1). An additional fixation with a mixture of methanol:acetic acid (95:5) for 10 min at -20°C was performed when using this antibody according to the manufacturer (Dumoulin et al., 2001).

NeuN

NeuN purified monoclonal antibody A60 (IgG1) was raised in mouse and apparently labels all spinal neurons in rats too (Todd et al., 1998). This antibody used in our experiments reveals a similar immuroreactivity pattern in the rat MDH (see Fig. 5) compared with DH (Todd et al., 1998). The immunogen was purified cell nuclei extracted from mouse brain. This antibody recognizes mostly nuclear antigens and weakly cytoplasm ones (Mullen et al., 1992; Wolf et al., 1996). This antibody reveals three bands in the 46-48 kDa region on Western blot analysis and binds to DNA *in vitro* (Mullen et al., 1992). It recognizes neither glia cells nor non neuronal tissue. No staining is observed when the primary antibody is replaced by normal serum in mouse (Lorenzo et al., 2008).

PKCγ

PKCγ affinity purified polyclonal antibody (C-19) was raised in rabbit and recognizes an epitope located within the amino acid residues 679-697 at the C-terminal variable (V5) region

of the PKCγ. A mouse synthetic peptide, Asp-Phe-Val-His-Pro-Asp-Ala-Arg-Ser-Pro-Thr-Ser-Pro-Val-Pro-Val-Pro-Val-Met, corresponding to these amino acid residues 679-697 of PKCγ was used as immunogen. This antibody reveals two closely spaced bands of the appropriate molecular weight (80 kDa) on Western blot analysis of brain lysates (Cardell et al., 1998). Immunoreactivity is observed within the lamina II_i of mouse DH (Malmberg et al., 1997), rat MDH (Fig. 2; Miraucourt et al., 2007) but not of $PKC\gamma^{-/-}$ mouse DH (Malmberg et al., 1997). Staining is completely abolished when the antiserum is preabsorbed for 30 min with 40 $ng.ml^{-1}$ of the mouse PKCγ peptide (Fig. 2A).

PKCγ monoclonal antibody PK-G4 (IgG2a) was raised in mouse and recognizes an epitope located within the amino acid residues 684-697 at the C-terminal variable (V5) region of the PKCγ. A synthetic peptide, Cys-Asp-Ala-Arg-Ser-Pro-Thr-Ser-Pro-Val-Pro-Val-Pro-Val-Met, corresponding to the amino acid residues 684-697 of PKCγ was used as immunogen. This antibody reveals the band of the polypeptide PKC (80 kDa) on Western blot analysis of brain lysates in wild type but not in $PKC\gamma^{-/-}$ mice (Yevseyenkov et al., 2009). It shows a unique immunostaining in lamina II_i of MDH (Fig. 2C) where PKCγ is known to be restricted (Miraucourt et al., 2007). Stainings with the monoclonal and polyclonal antibodies fully overlap (Fig. 2D).

VGLUT3

The vesicular glutamate transporter 3 (VGLUT3) polyclonal antibody was raised in guinea-pig and was generously provided by Dr. H. Hioki (Kyoto university, Japan). It was affinity-purified with antigen-conjugated column. This antibody recognizes an epitope located within amino acid residues 564-588 at the C-terminal region of the VGLUT3 antigen in mouse and rat brain tissue using immunoblotting and imunohistochemistry. It shows a unique immunostaining in the lamina II_i of MDH (Fig. 7) where VGLUT3 is known to be restricted

(Seal et al., 2009). Using this antibody, no immunoreactivity is observed in VGLUT3$^{-/-}$ mice (Nakamura et al., 2004; Seal et al., 2009).

The specificity of antibodies was also verified by omitting either primary or secondary antibodies (data not shown). In those cases, no staining was visualized confirming the appropriate dilution and specificity of antibodies used in this study.

Protein extraction and Western blot

Lumbar spinal cord or brain tissue were homogenized by sonication in ice-cold buffer (buffer RIPA containing 1% NP-40, 0.5% sodium Deoxycholate and 0.1% of Sodium Dodecylsulfate) containing protease inhibitors (Roche SAS, Boulogne-Billancourt, France). After 30 min at 4°C in rotating wheel, the mix was centrifuged at 14 000 rpm for 15 min. The supernatants were collected and quantified by the Lowry method (Bio-Rad DC Protein Assay, Marnes-la-Coquette, France).

Total proteins were subjected to SDS-PAGE electrophoresis on 10% polyacrylamide gels. Membranes were incubated overnight at 4°C with mouse anti-$GABA_A$ receptor antibody (1/500) or with mouse anti-Glycine receptor antibody (1/1000). Immunoreactivity was detected using polyclonal goat anti-mouse immunoglobulins-HRP (DakoCytomation, Glostrup, Denmark). Controls were incubated without primary antibody. Bands were visualized by using a chemiluminescent detection system (luminata, Millipore, Molsheim, France). Pictures of the blots were taken with a ChemiGenius 2XE apparatus under the control of GeneSnap program (Syngene, Cambridge, UK).

Immunohistochemistry

Rats were deeply anaesthetized with urethane (1.5g/kg i.p.) and transcardially perfused with ice-cold 0.1 M phosphate buffer saline, pH 7.4 (PBS) followed by ice-cold 4%

paraformaldehyde (PFA) diluted in PBS. Brainstem was quickly removed and immersed into fixative solution for 2 h at 4°C before cryoprotection in 30% sucrose in PBS for 48 h at 4°C. Forty µm coronal sections were cut on a freezing microtome and collected in PBS before being processed. Free floating sections were first treated with 50 mM NH_4Cl diluted in PBS for 30 min at room temperature (RT). After several washes in 0.1 M PBS with 0.2% Triton (PBS-Tx), sections were blocked by pre-incubation in 5% Normal Goat Serum (NGS) in PBS-Tx for 1 h at RT. After washes in PBS-Tx, sections were incubated with a primary antibody diluted in 5% NGS in PBS-Tx for 24 h at 4°C. Sections were then washed with 5% NGS followed by washes in PBS-Tx. Tissues were incubated with secondary fluorescent antibody diluted in 5% NGS in PBS-Tx for 1 h at RT. Finally, sections were washed in 5% NGS, in PBS-Tx and then in PBS. Sections were transferred onto gelatinized slides before being coverslipped with DPX mountant for histology. Neurons containing VGLUT3, NeuN, $GABA_A$ receptor, glycine receptor and/or PKCγ immunoreactivity in the MDH were first photographed using a fluorescent Zeiss Axioplan 2 Imaging microscope coupled with a Hamamatsu C4742–95 digital camera, by switching between FITC and Rhodamine filter sets at respectively x5 and x20 magnifications before being analyzed with a confocal microscope. The delineation of the MDH was based upon the Paxinos and Watson atlas (Paxinos and Watson, 1997) and our own myeloarchitectural atlas as determined by our previous work (Miraucourt et al., 2011).

For control of PKCγ antibody specificity, MDH sections were cut in contralateral and ipsilateral hemisections and incubated into either primary antibody preabsorbed with 40 $ng.ml^{-1}$ of PKCγ synthetic peptide (Santa Cruz Biotechnology p-sc-211, CA) 30 min at RT or with primary antibody alone as described above.

Confocal laser scanning microscopy

Sections were analyzed with a Zeiss LSM 510 confocal laser scanning microscope by using 488- and 543-nm excitation laser light. In order to suppress emission cross-talk, the microscope was configured to perform all scanning in sequential mode. Z-series were scanned at x20 and x63 magnifications with an oil immersion lens and a z-step of 0.37 µm. The z-series were first examined with the Zeiss LSM image examiner©. Each image was then analyzed with Fiji-ImageJ 1.47 program (http://rsbweb.nih.gov/ij ; Schindelin et al., 2012). For fluorescence pattern analysis, a single image corresponding to the z-middle of cell was quantified using plot profile analysis plug-in. For this, a single line going from either side of the neuron thought the plasma membrane, cytoplasm and nucleus was traced and grey values calculated. The relative changes in fluorescence intensity were measured from the background level and plasma membrane and cytoplasm separated considering the limited resolution of light. To ensure that the analyzed neurons were entirely included in the z-section, 3D-reconstruction was systematically performed using the 3D-viewer plug-in (Schmid et al., 2010) after cropping an isolated neuron.

Electron microscopy (pre-embedding method)

Animals were deeply anesthetized with pentobarbital and perfused through the ascending aorta with an ice-cold fixative containing 4% PFA, 1.5% picric acid and 0.1% glutaraldehyde diluted in 0.1 M phosphate buffer, pH 7.4 (PB). Brainstem was rapidly dissected out and postfixed in the same fixative without glutaraldehyde for 2 h and then rinsed in 0.1 M PBS, pH 7.4 at 4°C overnight. Free-floating sections (40-µm thickness) were obtained on a Vibratome (Leica, Nanterre, France) and permeabilized 30 min with 1% borohydride diluted in 0.1 M PBS. After several washes in 0.1 M PBS, sections were then saturated 30 min at RT with 1% Bovine Serum Albumin (BSA) diluted in 0.1 M Tris, 0.15 M NaCl and 0.05 % Tween (TNT). For single immunostaining, sections were first incubated overnight at 4°C with

the primary antibody diluted in TNT with 1% BSA. After several washes with TNT, sections were incubated for 2 h at RT with the secondary antibody diluted in TNT with 1% BSA followed by a Diaminobenzindine (DAB) reaction. For immunogold reaction, sections were pre-treated with 1% glutaraldehyde diluted in distilled water 10 min at RT followed by several washes with TNT. A silver amplification was performed with HQ SILVER Nanoprobes (Yaphank, NY, USA). In all cases, sections were post-fixed for 1 h in dark with 1% OsO_4 diluted in PB after several washes in PB. Sections were then dehydrated through a graded series of ethanol (10 min in 50% ethanol, 10 min in 70% ethanol, 2 x 15 min in 95% ethanol, 2 x 20 min in 100% ethanol and 2 x 30 min in propylene oxide). Sections were embedded by the progressive temperature lowering technique. Briefly sections were incubated for 2 h at RT with 50% EPON resin and 50% propylene oxide, overnight with 100% EPON resin, 4 h at RT with freshly-made EPON resin and then 36 h at 60 °C. Ultrathin sections (60–100 nm) from blocs were mounted on gold mesh grids and observed under a HITACHI H7650 electron microscope. For double immunostainings, DAB reaction was performed immediately after Silver amplification and several washes with distilled water.

For sampling, lamina II_i containing embedded blocs were first cut by visualizing the dark PKCγ immunoreactive band formed by DAB reaction. Selected blocs were then mounted onto an ultramicrotome to be cut in ultrathin sections. For sections stained by gold particles, no visual immunoreactivity could be used to select lamina II_i. Therefore, embedded blocs were first cut according to the relative distance of lamina II_i to the Lissauer tract (≈ 65 µm) before being mounted onto an ultramicrotome to be cut in ultrathin sections. Serial sections were mounted onto gold mesh grids, each grid containing a distant focal plane. Only the most immunoreactive ultrathin section was selected in each grid to avoid repetitive analysis. Because the number of immunoreactive profiles can vary from one ultrathin section to

another, the number of sections used for each rat was determined so that the number of immunoreactive profiles was similar in the three independent rat samples.

Cell counting

NeuN and/or PKCγ immunoreactive cells in the MDH were first scanned at x20 magnification and analyzed using Fiji-ImageJ 1.47 program. Sections were analyzed at -1200 µm from the obex aperture, i.e. at about the middle of the rostro-caudal extend of MDH (Strassman and Vos, 1993; Miraucourt et al., 2011), for each rat (n=4). For cell counting, a 300 x 400 µm window was positioned so that its median axe was perpendicular to the MDH border and its dorsolateral end at the border between the white and grey matter (Lorenzo et al., 2008). In addition, the center of this window was on the diagonal of a rectangle enclosing the whole MDH (see Fig. 3). NeuN and PKCγ immunoreactivity profiles were counted separately using the cell counter plug-in. Delimitation of laminae borders was first done using merged NeuN/PKCγ images. The border between lamina I and lamina II_o was delimited so that the lamina I contained the apparent unicellular layer of characteristic large lamina I output neurons. The border between lamina II_o and lamina II_i was set based on the apparition of a dense PKCγ immunoreactive neuropil and that between lamina II_i and III_o on the disappearance of this neuropil. As we did not use neurochemical markers to delineate the border between lamina III and IV (Polgar et al., 2006), we did not separate these two last laminae. A cell was counted as immunopositive if (1) immunostaining of a single cell was clearly defined, (2) its level was at least two times that of the background levels, and (3) it had disappeared at both the top and bottom surfaces of z-stack. To ensure that a cell was not counted several times, the immediate look-up z-section was used as reference and compared to the subsequent z-section. 3D reconstruction using the 3D-viewer plug-in was also used to compare our counting with the representative neuronal structure reconstructed from the z-

series. If any doubt was present, cells were reanalyzed at a higher magnification using x63 oil immersion lens.

Data and statistical analysis

Rostro-caudal levels of the MDH are shown as distance in µm from the obex aperture. VGLUT3-immunoreactive fibers were analyzed using Fiji-ImageJ 1.47 program and the simple neurite tracer plug-in (Longair et al., 2011) in superficial layers of the MDH within the section -1200 µm from the obex aperture. Because (1) the intensity of immunoreactivity can vary from one sample to another and (2) lamina width is not even in the MDH, we did not assessed fluorescence intensity in each lamina. Rather, pictures from neurolucida reconstructions were digitized. The area of VGLUT3 immunoreactivity was quantified using Fiji-ImageJ 1.47 program and normalized to the total area of the respective lamina. For electron microscopy, immunogold particles were analysed using Fiji-ImageJ 1.47 program and PointDensity or DistToPath plug-in as previously described (Larsson et al., 2001). Distances between the midpoint of each gold particle signaling $GABA_A$ receptor, glycine receptor or PKCγ immunoreactivity and the centre line of the associated plasma membrane or the middle of the synaptic cleft were measured. Areal densities (number of particles per μm^2) were also computed. Subcellular compartmentation of PKCγ-immunoreactivity in MDH and cerebellar neurons was normalized to the total fluorescence of the cell. Values are expressed as mean ± SEM. All quantitative analyses, graphs and statistical tests were performed on GraphPad Prism™, version 5.0. For statistical analyses, we used a one-way ANOVA followed by a Tuckey *post hoc*, after passed the Kolmogorov-Smirnov normality test. In all cases, $p<0.05$ was considered as statistically significant. Pictures were optimized for visual quality using Fiji-ImageJ 1.47 program at the end of analysis. Figures were made using CorelDRAW© 12.

RESULTS

Distribution of PKCγ interneurons within the spinal trigeminal nucleus

In the spinal trigeminal nucleus, PKCγ immunoreactivity was found exclusively within the MDH (Fig. 4B-E) where it formed a continuous, homogeneous and dense band in superficial laminae from the dorsomedial to the ventrolateral part in transverse sections. Actually, such PKCγ immunoreactive band varied throughout the rostro-caudal axis of the MDH. Rather large at the caudal end of the MDH (thickness at -2400 μm: 65.6 ± 2.3 μm, n = 5), this band progressively narrowed (-800 μm: 36.1 ± 0.7 μm, n = 5), became scattered (between -400 and 0 μm; corresponding to the transition from the MDH to subnucleus interpolaris (Sp5I), and finally vanished (at +400 μm), where both MDH and Sp5I overlap and laminar organization has disappeared (Fig. 4A).

At low magnification, PKCγ immunoreactivity appeared as mainly a dense neuropil with few strongly immunoreactive cell bodies and associated dendrites in lamina II_i. However, though most immunoreactive neurons were located within this lamina II_i neuropil, there were also stained cells in lamina I, lamina II_o, and outer lamina III (Fig. 5B, D). As previously observed (Polgar et al., 1999), PKCγ immunoreactivity was weaker in the more dorsal (lamina I and II_o) than in the more ventral cells (lamina II_i and III). When sections immunostained with both PKCγ and NeuN were viewed at high magnification (Fig. 5C), the vast majority of PKCγ immunoreactive cells (92 ± 3%) were found to be NeuN-positive, indicating that these were neurons.

Quantitative analysis of NeuN immunoreactivity indicates that lamina II exhibits the most intense neuronal density, especially at its dorsal part (47 ± 4 and 34 ± 4 neurons /100 μm^2 in lamina II_o and II_i, respectively, compared with 14 ± 4 and 24 ± 2 neurons /100 μm^2, in lamina I and III-IV, respectively) as already observed in spinal DH (Todd et al., 1998; Polgar et al.,

2004) (Fig. 5A). Most of PKCγ-immunoreactive neurons were located within lamina II_i (52 ± 6%) where they represent 30 ± 5% of the total number of neurons within this lamina (Fig. 5D, E). Results of this study are shown in Table 4. As PKCγ immunoreactivity is predominantly found in lamina II_i, we will focus on PKCγ- immunoreactive interneurons in lamina II_i of the MDH in the remainder of the paper.

Synaptic inputs to lamina II_i PKCγ interneurons

We performed a transmission electron microscopy study of synapses on PKCγ-immunoreactive interneurons. A total 199 synaptic appositions were analyzed, 46 on somatic and 153 on dendritic PKCγ-immunoreactive profiles. Most of them (67%) were asymmetric (likely excitatory), almost exclusively (96%) axo-dendritic synapses, whereas 33% were symmetric (likely inhibitory), mostly axo-somatic ones (62%) (Fig. 6 and Table 5). Out of the 128 analyzed axo-dendritic asymmetric synapses on PKCγ immunoreactive interneurons, only 20 (16%) were between large primary afferent terminals and these neurons (Fig. 6 and Table 5).

In mice, C-LTMRs have been shown to specifically express the vesicular glutamate transporter 3 (VGLUT3) and terminate in lamina II_i, precisely within the PKCγ immunoreactive band (Seal et al., 2009; Li et al., 2011). To examine whether C-LTMRs directly terminate on PKCγ immunoreactive neurons, we performed a light and electron microscopy double labeling study of MDH sections with VGLUT3 and PKCγ antibodies. Our light microscopy study confirmed that, in rats too, VGLUT3 immunoreactive fibers terminate mostly in lamina II_i. They travel from the Lissauer tract to lamina II_i in a dorso-ventral direction and form a dense plexus within this lamina where PKCγ immunoreactivity is predominantly located (Fig. 7A-C). Indeed, VGLUT3 immunoreactivity was significantly higher in lamina II_i compared to lamina I ($p < 0.001$, $n = 5$), II_o ($p < 0.001$, $n = 5$) and III_o ($p <$

0.01, n = 5) (Fig. 7C). This raises the question as to whether VGLUT3-immunoreactive fibers form synapses onto PKCγ interneurons. To address this question, altogether, 17 somatic and 167 dendritic PKCγ immunoreactive profiles in 3 rats were analyzed at the electron microscopy level. Somewhat surprisingly, though, no synaptic contact between VGLUT3 immunoreactive terminals and PKCγ-immunoreactive interneurons could be found Finally, we observed only one morphological type of primary afferents terminals onto PKCγ-immunoreactive neurons. Out of the 20 afferents that terminated onto PKCγ-immunoreactive interneurons, we quantitatively analyzed 15 terminals that could be entirely observed and clearly delineated under the electron microscopy. These were large terminals (section area: 2.55 ± 0.43 μm^2, n = 15) with light axoplasm containing loosely packed, uniformly clear vesicles and numerous mitochondria (3.64 ± 0.29 per μm^2, n = 15) and forming the central element of synaptic glomeruli of type II (Ribeiro-da-Silva and Coimbra, 1982) (Fig. 7D). Such terminals are thought to be endings of myelinated primary afferent fibers (Ribeiro-da-Silva and Coimbra, 1982; Maxwell and Réthelyi, 1987; Larsson and Broman, 2005; Neumann et al., 2008). Interestingly, neither large dense core vesicle terminals nor synaptic glomeruli of type I, which are assumed to be the endings of unmyelinated peptidergic and IB4 primary afferent terminals, were found on PKCγ-immunoreactive interneurons. Together with our failure to find any VGLUT3-immunoreactive boutons on PKCγ-immunoreactive interneurons, these observations strongly suggest that neither nociceptive nor tactile unmyelinated C-fibers terminals terminate on lamina II_i PKCγ immunoreactive neurons.

It was recently shown that PKC-immunoreactive interneurons receive direct glycinergic synaptic inhibition (Miraucourt et al., 2007). Do lamina II_i PKCγ interneurons receive pure glycinergic synaptic inhibition? To address this question, we assessed glycinergic and $GABA_A$ergic receptor immunoreactivity on lamina II_i PKCγ-immunoreactive interneurons, at the electron microscopic level. Altogether, 7 somatic and 20 dendritic PKCγ-immunoreactive

profiles were analyzed for $GABA_A$ receptor immunoreactivity and an additional 7 somatic and 20 dendritic PKCγ-immunoreactive profiles, for glycine receptor immunoreactivity. The sizes of these PKCγ-immunoreactive somatic and dendritic profiles were the same in the two series of experiments: 33.7 ± 4.0 μm^2 and 2.5 ± 0.6 μm^2 compared with 42.5 ± 5.9 μm^2 and 3.2 ± 1.1 μm^2 for $GABA_A$ and glycine receptor-immunoreactive somatic and dendritic profiles, respectively. Altogether, 433 gold particles signaling $GABA_A$ receptor immunoreactivity (Fig. 8) and 515 ones signaling glycine receptor immunoreactivity (Fig. 9) were registered on PKCγ-immunoreactive interneurons. $GABA_A$ or glycine receptor immunoreactivity was found on all PKCγ-immunoreactive somas (Fig. 8A and 9A) and most, but not all, PKCγ-immunoreactive dendrites. Indeed, no gold particle for $GABA_A$ and glycine receptor immunoreactivity could be registered on 7 (Fig. 8E) and 6 (Fig. 9E) PKCγ-immunoreactive dendrites, respectively. A quantitative analysis was performed to investigate the precise distribution of gold particles signaling $GABA_A$ and glycine receptor immunoreactivities to the plasma membranes of PKCγ-immunoreactive interneurons (Fig. 8B-E and 9B-E). This distribution indicates that $GABA_A$ and glycine receptors are localized primarily to plasma membranes and the underlying cytoplasm. About half of gold particles signaling $GABA_A$ and glycine receptor immunoreactivities are found within 400 nm of somatic (Fig. 8B,C and 9B,C) and 100 to 150 nm of dendritic (Fig. 8D and 9D) plasma membranes. Consistent with this, when gold particles signaling $GABA_A$ and glycine receptor immunoreactivities are registered on PKCγ-immunoreactive dendrites, the areal density of gold particles in dendrites is higher than that in somas (Fig. 8E and 9E). It is noteworthy that $GABA_A$ and glycine receptor immunoreactivities were also found within cytoplasm and, to a lesser extent, nuclei. This particular localization of inhibitory receptors suggests a dynamic expression at the neuronal membrane with their different states (active, biosynthesized or recycled).

Subcellular localization of PKCγ immunoreactivity within lamina II_i interneurons

PKCγ primary antibody combined with HRP-conjugated secondary antibody revealed two types of morphologically distinct PKCγ-immunoreactive interneurons: fusiform and oval-shaped (Fig. 10A, B). The size of their soma, measured by confocal microscopy, is 13.1 ± 0.8 x 6.5 ± 0.3 and 9.1 ± 0.4 x 7.4 ± 0.4 µm for fusiform (n = 10) and oval-shaped (n = 10) neurons, respectively. Immunoreactivity is found in the somatic and dendritic cytoplasm and, to a lesser extent, in the nucleus. At high magnification, though DAB reaction product can be found throughout the cytoplasm, it appears to be localized primarily to, or close to, the plasma membrane (Fig. 10A, B). This suggests that PKCγ is mostly associated with plasma membranes.

To further assess the subcellular distribution of PKCγ, we used the quantitative electron microscopy immunogoldcytochemistry. Altogether, 267 particles signaling PKCγ were registered on 8 dendrites (3 rats) (Fig. 10 C, D), being exclusively postsynaptic (see examples in Fig. 10 C, E). A first quantitative analysis was performed to assess the distribution of gold particles signaling PKCγ immunoreactivity to plasma membranes (Fig. 10 D). The density of gold particles peaks at 30 nm from plasma membranes. Thus, 56.6 ± 6.6% of gold particles are within 30 nm of plasma membranes (corresponding to the experimentally determined maximum epitope–gold particle–centre distance (Matsubara et al., 1996)) and 77.2 ± 5.3% within 50 nm. A second quantitative analysis examined the distribution of gold particles signaling PKCγ immunoreactivity to synaptic active zones (Fig. 10 F). Gold particles appear to preferentially cluster close to, but not within, the synaptic space (distance from synaptic clefts: 248 ± 11 nm; 182 particles, 15 synapses, 3 rats) (Fig. 10 E, F). Moreover, presumably endosomal vesicles highly stained with gold particles, were often found close to the synaptic space (see examples in Fig. 10 C, E).

Most gold particles for PKCγ immunoreactivity are closely associated with plasma membranes in lamina II_i interneurons. It is now well established that activation of glutamate receptors and the consecutive increase in cytosolic free Ca^{2+} promotes a quick translocation of PKC for the cytoplasm to plasma membranes (Vaccarino et al., 1987; Sakai et al., 1997; Oancea et al., 1998; Oyasu et al, 2008). This raises the question as to whether the preferential localization of PKCγ to plasma membranes actually results from a redistribution of the enzyme following glutamate release during the initiation of the perfusion procedure. To address this question, we compared the subcellular localization of PKCγ immunoreactivity in MDH PKCγ-immunoreactive interneurons with that in cerebellar Purkinje cells, which are known to also highly express PKCγ. In baseline conditions, PKCγ is located within the cytoplasm of these Purkinje cells and translocates to plasma membranes upon activation (Sakai et al., 1997; Sakai et al., 2004). Using light microscopy, we assessed the sub-cellular localization of PKCγ-immunoreactivity in both trigeminal PKCγ-immunoreactive interneurons (n = 10) and cerebellar Purkinje cells (n = 10) in naive animals. In MDH neurons, PKCγ immunoreactivity is mainly located in plasma membranes (Fig. 11A, empty arrow head) and to a lesser extent in the cytoplasm (Fig. 11A, filled arrowhead) and nucleus (Fig. 11A, arrow). On the other hand, PKCγ immunoreactivity in cerebellar Purkinje cells is equally located in the cytoplasm (Fig. 11C, filled arrowhead) and plasma membranes (Fig. 11C, empty arrow head) and little, if none, in the nucleus (Fig. 11C, arrow). Quantitative analysis of gray levels in the different compartments of both trigeminal and cerebellar PKCγ immunoreactive cells, using confocal microscopy, confirmed that PKCγ immunoreactivity is predominantly located in plasma membranes in trigeminal interneurons (Fig. 11 B, E, F), but in both plasma membranes and cytoplasm, in cerebellar Purkinje cells (Fig. 11 D, E, G). These results thus suggest that the localization of PKCγ on plasma membranes in baseline conditions is a specific feature of trigeminal interneurons. However, clearly, trigeminal

PKCγ-immunoreactive neurons and cerebellar Purkinje cells exhibit many other morphological differences including size and nucleus/cytoplasm ratio (Fig. 11 B, D).**DISCUSSION**

Using light and electron microscopy, our anatomical and morphological study shows that PKCγ immunoreactivity is restricted to a single subnucleus in the spinal trigeminal nucleus: the MDH. Within MDH, PKCγ-immunoreactive neurons are concentrated in superficial laminae, mostly in lamina II_i, where they constitute 1/3 of the total number of neurons. The majority of synapses on lamina II_i PKCγ-immunoreactive interneurons are asymmetric (likely excitatory). However, neither large dense core vesicle-containing boutons nor VGLUT3-immunoreative ones, which are both specific of unmyelinated afferents, could be found forming contacts with lamina II_i PKCγ$^-$immunoreactive interneurons. Lamina II_i PKCγ$^-$immunoreactive interneurons receive both $GABA_A$ergic and glycinergic inputs. At the subcellular level, PKCγ immunoreactivy within lamina II_i MDH neurons is mostly concentrated on plasma membranes, close to (but not within) postsynaptic densities, in baseline conditions. Such subcellular localization is thus very different from that in Purkinje cells where PKCγ immunoreactivy is mostly cytoplasmic in the same conditions.

Technical considerations

We used a modification of the physical dissector method (Williams and Rakic, 1988; Coggeshall, 1992; Guillery, 2002; Polgar et al., 2004; Polgar et al., 2011) to provide an unbiased count of neurons. However, MDH is a heterogeneous structure which can vary in length and width throughout its rostro-caudal axis. A precise estimate of the total number of neurons that exist in this structure is therefore not possible. Nevertheless, to allow comparison with other studies, we report here densities of neurons in each MDH lamina at level -1200 μm.

As previously described both in the spinal (Mori et al., 1990; Malmberg et al., 1997; Polgar et al., 1999) and medullary DHs (Li et al., 2001b; Miraucourt et al., 2007), PKCγ immunoreactivity forms a dense plexus – consisting of cell bodies and associated dendrites within lamina II_i. In addition, as in spinal DH (Polgar et al., 1999), PKCγ-immunoreactive cells can also be found within lamina I, II_o and III in the MDH. Nevertheless, PKCγ-immunoreactive cells within both lamina II_o and III are actually located close to the borders of lamina II_i. Li et al. (2001b) reported that, in MDH, PKCγ-immunoreactive cells are most prominent in lamina II, but in its outer part. The apparent discrepancy in the laminar localization of the band of strong PKCγ immunoreactivity between this and ourstudy probably reflects a slight difference in the placing of the lamina II/III border between the two studies.

PKCγ neuronal population

Double immunostaining with PKCγ and NeuN antibodies reveals that the great majority of PKCγ immunoreactive cells are also NeuN-positive indicating that they are neurons. That some PKCγ immunoreactive cells are NeuN-negative raises the possibility that few PKCγ immunoreactive cells are not neurons. This is very unlikely as PKCγ has been shown to be expressed solely in neurons (Kose et al., 1988). Furthermore, no PKCγ immunoreactive glia cells were found at the electron microscopy level in our study. Finally, it has already been noted that some neurons might be NeuN-negative (Lorenzo et al., 2008).

Cell counts reveal that about half of PKCγ-immunoreactive neurons within MDH are restricted to lamina II_i where they constitute 1/3 of the total number of neurons. Thus, taken together with previous estimates that the great majority of PKCγ-immunoreactive neurons are excitatory (Martin et al., 1999; Polgar et al., 1999) and that nearly 70% of neurons in lamina II_i are excitatory (Polgar et al., 2003), the present study indicates that PKCγ-immunoreactive neurons make up around 50% of the excitatory neurons in lamina II_i. Lamina II_i PKCγ-

immunoreactive interneurons would thus constitute one of the relatively largest population of neurons within one lamina of the medullary, and likely spinal, DHs. Preprotachykinin B (PPTB) immunoreactive neurons have also been shown to be highly concentrated in lamina II_i where they constitute 16% of the neurons (Polgar et al., 1999). However most of PPTB immunoreactive neurons (76%) also express PKCγ suggesting that these are the same neurons.

PKCγ immunoreactivity varies between cells with most lamina II_i PKCγ-immunoreactive neurons being more immunoreactive than those within other laminae, in both the medullary (present results) and spinal DHs (Polgar et al., 1999). Several subpopulations of PKCγ-immunoreactive neurons can be identified based on the intensity of PKCγ immunoreactivity and expression of various neurochemical markers. For example, PKCγ-immunoreactive neurons which express PPTB are weakly to moderately PKCγ immunoreactive (Polgar et al., 2006) whereas those expressing neurotensin and somatostatin are moderately to strongly PKCγ immunoreactive (Polgar et al., 1999). Since neurotensin and somatostatin are expressed in different sets of excitatory interneurons (Polgar et al., 1999; Polgar et al., 2006), neurotensin- and somatostatin-expressing PKCγ-immunoreactive neurons may represent two different populations of PKCγ-immunoreactive neurons. Similarly, AMPA receptor subunit glutamate 2/3 is expressed by only 50% and calbindin, by 15-25% of PKCγ-immunoreactive neurons (Hughes et al., 2008). Moreover, a basic distinction can be drawn between PKCγ-immunoreactive neurons within and outside lamina II_i. Thus, AMPA receptor subunit glutamate 1 are present on 1/3 of PKCγ-immunoreactive neurons in lamina I and II_o but on very few in lamina II_i (Hughes et al., 2008). Similarly, PKCγ-immunoreactive neurons in lamina I and III can express NK1 receptors while there is essentially no co-expression of PKCγ and NK1 receptor in lamina II_i (Polgar et al., 1999; Hughes et al., 2008). This last

distinction might be associated with particular functional types as PKCγ immunoreactive neurons in lamina I and III, but not in lamina II, can project to the thalamus (Li et al., 2001b). Therefore, the differential expression of PKCγ immunoreactivity and the detection of various neurochemical markers strongly suggest that there are different subpopulations of PKCγ-immunoreactive neurons with, likely, different functions. We therefore concentrated on PKCγ-immunoreactive interneurons in lamina II_i for the rest of our study.

Primary afferent inputs to PKCγ-immunoreactive interneurons

In mice, C-LTMR, terminate in lamina II_i, precisely within the PKCγ immunoreactive band (Seal et al., 2009; Li et al., 2011). The present study confirms that, in rats, too, VGLUT3 immunoreactivity is concentrated within lamina II_i where about half of PKCγ interneurons are located. Nervertheless, at the electron microscopic level, despite our efforts, no bouton containing VGLUT3 could be found forming synapse with PKCγ-immunoreactive interneurons. It is then more likely that VGLUT3 containing afferents actually terminate on another population of lamina II_i interneurons, namely calbindin-positive interneurons, which have been shown to receive unmyelinated, but not myelinated, primary afferents (Braz and Basbaum, 2009). It has to be noted, however, that C-LTMRs and PKCγ interneurons appear to be both involved in injury- or inflammation-induced secondary mechanical allodynia, the former transmitting the input that produces pain (Malmberg et al., 1997; Seal et al., 2009), suggesting that they are somehow functionally related.

Together with our failure to find any large dense core vesicle-containing terminals on PKCγ immunoreactive interneurons, these results suggest that PKCγ interneurons do not receive any unmyelinated but rather exclusively myelinated primary afferents. Such conclusion is consistent with previous evidence showing that central terminals that conduct in the Aβ range (Hughes et al., 2003) or contain the VGLUT1, the vesicular glutamate

transporter that is associated with large-diameter afferents (Neumann et al., 2008), contact PKCγ-immunoreactive interneurons in lamina II_i. In addition, a significant number of PKCγ$^-$ immunoreactive interneurons in lamina II_i are labeled by the transneuronal tracer wheat germ agglutinin when it is expressed in myelinated sensory neurons (Neumann et al., 2008; Braz and Basbaum, 2009). It has to be noted, however, that another type of LTMRs, namely thinly myelinated Aδ D-hair, terminates in lamina II_i and the outer part of lamina III (Maxwell and Réthelyi, 1987; Li et al., 2011). Since both Aβ and Aδ can form synaptic type II glomeruli in DH, our study cannot exclude the possibility that D-hairs directly contact PKCγ immunoreactive interneurons. Interestingly, activation of these two LTMRs leads to different pain symptoms (Treede and Magerl, 2000). In conclusion, different types of low threshold mechanoreceptors might thus engage different types of lamina II_i neurons, the myelinated ones, the PKCγ interneurons and the unmyelinated ones, the calbindin interneurons.

Inhibitory receptors onto PKCγ-immunoreactive interneurons

Our electron microscopic study shows that both glycine and $GABA_A$ receptors are expressed in lamina II_i PKCγ interneurons in adult rats. Evidence for glycine receptor immunoreactivity on lamina II_i PKCγ-immunoreactive interneurons had already been obtained (Miraucourt et al., 2007). The present study demonstrates in addition that $GABA_A$ receptors are also present on lamina II_i PKCγ-immunoreactive interneurons. This is consistent with anatomical evidence showing that lamina II_i PKCγ interneurons receive many vesicular GABA transporter-containing boutons, including those from neuropeptide Y GABAergic interneurons (Polgar et al., 2011). The electrophysiological observation that pure glycine receptor- and pure $GABA_A$ receptor-mediated events can be recorded in the same lamina II neuron and the fact that benzodiazepine can convert many pure glycine receptor-mediated events into mixed glycine receptor-$GABA_A$ receptor-mediated events (Keller et al., 2001)

suggests the existence of a heterogeneous junctional distribution of glycinergic and $GABA_A$ergic receptors in laminas II neurons. However, because of technical limits including an overlap between electron-dense DAB product and gold particles in the plasma membrane due to a pre-embedding approach used in this study, we cannot address the issue of the pattern of distribution of glycinergic and $GABA_A$ergic receptors in symmetric synapses formed onto lamina II_i PKCγ-immunoreactive interneurons. Also, it has to be noted that we might quantitatively underestimate the presence of both $GABA_A$ and glycine receptors at the cell membrane, including the synaptic cleft. Indeed, using a pre-embedding approach, monoclonal antibodies raised against the extracellular domain of $GABA_A$ and glycine receptors might not have reached the epitope because the narrow extracellular space preventing either the primary antibody or the 1.4-nm gold particle-coupled secondary antibody to enter the synaptic cleft (Zerari et al., 1998).

Subcellular localization of PKCγ

PKCγ, a conventional PKC isoform, is known to be translocated from the cytosol to plasma membranes when activated by Ca^{2+} and diacylglycerol (Sakai et al., 1997; Oancea et al., 1998). Therefore, the translocation of PKCγ can be considered as a good marker of whether this enzyme is activated or not. Our electron microscopic study of the subcellular localization of PKCγ immunoreactivity in lamina II_i interneurons of the MDH suggests that the enzyme is mostly located on, or very close to, plasma membranes. This result is consistent with previous electron microscopic studies in lamina IIi neurons within the spinal DH pointing out that, PKCγ immunoreactivity seems to be located on cell membranes in basal conditions, the reaction products being concentrated against the inner plasma membrane of dendrites (Mori et al., 1990; but see Martin et al., 2001). Since our result at the electron microscopic level showing that PKCγ immunoreactivity, by analysis of DAB reaction product

or immunogold particles, is predominantly located on plasma membranes in lamina II_i neurons implies that, in baseline conditions, most of the enzyme is activated, it was important to verify that this was not an experimental artifact. We performed two series of controls. We first investigated the subcellular localization of PKCγ immunoreactivity in lamina II_i interneurons using another technique, the confocal laser scanning fluorescent microscopy, and, then, compared it with that of Purkinje cells from the very same animals. On confocal images of PKCγ immunoreactivity in lamina II_i interneurons, fluorescence was predominantly located on plasma membranes. Interestingly, these images appear to be very similar to those of PKCγ immunostaining previously obtained in spinal DH where the most intense staining is clearly found at the membrane level (see Fig. 5-6 in Polgar et al., 1999 or Fig. 8-9 in Polgar et al., 2011). Moreover, using the very same confocal microscopy, we assessed PKCγ immunoreactivity in Purkinje cells from the same animals. Fluorescence appears to be rather uniformly distributed in the cytoplasm and plasma membranes, much the same as that of PKCγ fused with green fluorescent protein of transgenic mice before any stimulation (Sakai et al., 2004). This suggests that the preferential localization of PKCγ immunoreactivity on the plasma membranes of lamina II_i interneurons is a special feature of these neurons, both in medullary and spinal DHs. However, Cardell et al. (1998), using high resolution immunogold cytochemistry, found that, in Purkinje cells too, a large proportion of gold particles for PKCγ immunoreactivity is associated with plasma membranes. Nevertheless, comparison of the results obtained with fluorescent and electron-microscopy suggests that the preferential localization of PKCγ immunoreactivity on the plasma membranes of lamina II_i interneurons is a special feature of these neurons, both in medullary and spinal DHs. Nevertheless, it is noteworthy that the distance between the antibody-antigene site and gold particles can vary up to 30 nm (see Matsubara et al., 1996), and even more when using silver amplification.

Therefore, we cannot exclude the possibility that PKCγ is not located within but rather very close to plasma membranes.

PKCγ immunoreactivity, postsynaptic to asymmetric (excitatory) synapses, appears to cluster in the perisynaptic space at a distance of about 250 nm to the synaptic zone. Such distance corresponds to that of "synaptic molecules" (see Tardin et al., 2003), suggesting that PKCγ contributes to synaptic functions. Thus, PKCs appear to be involved in horizontal and vertical membrane-trafficking of glutamate receptors in many brain areas including DH (Li et al., 1999; Groc et al., 2004). And PKCγ itself has been shown to regulate synaptic plasticity in hippocampus (Abeliovich et al., 1993) as well as DH (Martin et al., 2001; Woolf, 2011).

In conclusion, our anatomical study establishes that PKCγ immunoreactivity is restricted to a single subnucleus within the spinal trigeminal nucleus: the MDH. No PKCγ immunoreactivity could be detected in the two other, more rostral, spinal trigeminal subnuclei: interpolaris and oralis. It is interesting to note that these three subnuclei exhibit very different anatomical organizations: only MDH includes laminae, much the same as those in spinal DH, and receives unmyelinated C-fiber primary afferents (Dallel et al., 1998; DaSilva and DosSantos, 2012). Lamina II_i PKCγ interneurons, at the border between noxious and innocuous tactile primary afferents, might thus regulate the cross-talk between sensory modalities. Receiving myelinated tactile primary afferent inputs, including Aβ, at the lamina II/III border, they would act as gateway of local excitatory circuits that mediate mechanical allodynia.

CONFLICT OF INTEREST STATEMENT

None of the authors has any conflict of interest to declare.

AKNOWLEDGMENTS

We thank A. Calas, E. Gontier, M. Petrel, S. Lacomme (Bordeaux Imaging Center), C. Blavignac, C. Szczepaniak (Centre Imagerie Cellulaire Santé), C. Vachias for expertise in image analysis, and A.M. Gaydier for secretarial assistance. We are grateful to Dr H. Hioki (Department of Morphological Brain Science Graduate School of Medicine, Kyoto University Konoe-cho, Japan) for the generous gift of the VGLUT3 antibody.

ROLE OF AUTHORS

All authors had full access to all the data in the study and take responsibility for the integrity of the data and the accuracy of the data analysis. Study concept and design: CP, ML and RD. Acquisition of data: CP, RB and SP. Analysis and interpretation of data: AA, CP, ML and RD. Drafting of the manuscript: AA, CP, and RD. Obtained funding: ML and RD. Study supervision: RD.

LITTERATURE CITED

Abeliovich A, Chen C, Goda Y, Silva AJ, Stevens CF, Tonegawa S. 1993. Modified hippocampal long-term potentiation in PKC gamma-mutant mice. Cell 75(7):1253-62

Basbaum AI, Bautista DM, Scherrer G, Julius D. 2009. Cellular and molecular mechanisms of pain. Cell 139(2):267-84.

Braz JM, Basbaum AI. 2009. Triggering genetically-expressed transneuronal tracers by peripheral axotomy reveals convergent and segregated sensory neuron-spinal cord connectivity. Neuroscience 163(4):1220-32.

Cardell M, Landsend AS, Eidet J, Wieloch T, Blackstad TW, Ottersen OP. 1998. High resolution immunogold analysis reveals distinct subcellular compartmentation of protein kinase Cγ and δ in rat purkinje cells. Neuroscience 82: 709–25.

Cheng HT, Suzuki M, Hegarty DM, Xu Q, Weyerbacher AR, South SM, Ohata M, Inturrisi CE. 2008. Inflammatory pain-induced signaling events following a conditional deletion of the N-methyl-D-aspartate receptor in spinal cord dorsal horn. Neuroscience 155(3):948-58.

Coggeshall RE. 1992. A consideration of neural counting methods. Trends Neurosci 15(1):9-13.

Dallel R, Dualé C, Molat JL. 1998. Morphine administered in the substantia gelatinosa of the spinal trigeminal nucleus caudalis inhibits nociceptive activities in the spinal trigeminal nucleus oralis. J Neurosci.18(10):3529-36.

DaSilva AF, DosSantos MF. 2012. The role of sensory fiber demography in trigeminal and postherpetic neuralgias. J Dent Res 91(1):17-24.

Dumoulin A, Triller A, Dieudonne S. 2001. IPSC kinetics at identified GABAergic and mixed GABAergic and glycinergic synapses onto cerebellar Golgi cells. J Neurosci 21(16):6045-57.

Groc L, Heine M, Cognet L, Brickley K, Stephenson FA, Lounis B, Choquet D. 2004. Differential activity-dependent regulation of the lateral mobilities of AMPA and NMDA receptors. Nat Neurosci 7(7):695-6.

Guillery RW. 2002. On counting and counting errors. J Comp Neurol 447(1):1-7.

Hughes AS, Averill S, King VR, Molander C, Shortland PJ. 2008. Neurochemical characterization of neuronal populations expressing protein kinase C gamma isoform in the spinal cord and gracile nucleus of the rat. Neuroscience 153(2):507-17.

Hughes DI, Scott DT, Todd AJ, Riddell JS. 2003. Lack of evidence for sprouting of Abeta afferents into the superficial laminas of the spinal cord dorsal horn after nerve section. J Neurosci 23(29):9491-9.

Keller AF, Coull JA, Chery N, Poisbeau P, De Koninck Y. 2001. Region-specific developmental specialization of GABA-glycine cosynapses in laminas I-II of the rat spinal dorsal horn. J Neurosci 21(20):7871-80.

Kose A, Saito N, Ito H, Kikkawa U, Nishizuka Y, Tanaka C. 1988. Electron microscopic localization of type I protein kinase C in rat Purkinje cells. J Neurosci 8(11):4262-8.

Larsson M, Broman J. 2005. Different basal levels of CaMKII phosphorylated at Thr286/287 at nociceptive and low-threshold primary afferent synapses. Eur J Neurosci 21(9):2445-58.

Larsson M, Persson S, Ottersen OP, Broman J. 2001. Quantitative analysis of immunogold labeling indicates low levels and non-vesicular localization of L-aspartate in rat primary afferent terminals. J Comp Neurol 430:147-159.

Li JL, Li YQ, Nomura S, Kaneko T, Mizuno N. 2001a. Protein kinase C gamma-like immunoreactivity in the substantia gelatinosa of the medullary dorsal horn of the rat. Neurosci Lett 311(3):185-8.

Li L, Rutlin M, Abraira VE, Cassidy C, Kus L, Gong S, Jankowski MP, Luo W, Heintz N, Koerber HR, Woodbury CJ, Ginty DD. 2011. The functional organization of cutaneous low-threshold mechanosensory neurons. Cell 147(7):1615-27.

Li P, Kerchner GA, Sala C, Wei F, Huettner JE, Sheng M, Zhuo M. 1999. AMPA receptor-PDZ interactions in facilitation of spinal sensory synapses. Nat Neurosci 2(11):972-7.

Li YQ, Li JL, Li H, Kaneko T, Mizuno N. 2001b. Protein kinase C gamma-like immunoreactivity of trigeminothalamic neurons in the medullary dorsal horn of the rat. Brain Res 913(2):159-64.

Loken LS, Wessberg J, Morrison I, McGlone F, Olausson H. 2009. Coding of pleasant touch by unmyelinated afferents in humans. Nat Neurosci 12(5):547-8.

Longair MH, Baker DA, Armstrong JD. 2011. Simple Neurite Tracer: open source software for reconstruction, visualization and analysis of neuronal processes. Bioinformatics 27(17):2453-4.

Lorenzo LE, Ramien M, St Louis M, De Koninck Y, Ribeiro-da-Silva A. 2008. Postnatal changes in the Rexed lamination and markers of nociceptive afferents in the superficial dorsal horn of the rat. J Comp Neurol 508(4):592-604.

Malmberg AB, Chen C, Tonegawa S, Basbaum AI. 1997. Preserved acute pain and reduced neuropathic pain in mice lacking PKCgamma. Science 278(5336):279-83.

Martin WJ, Liu H, Wang H, Malmberg AB, Basbaum AI. 1999. Inflammation-induced up-regulation of protein kinase Cgamma immunoreactivity in rat spinal cord correlates with enhanced nociceptive processing. Neuroscience 88(4):1267-74.

Martin WJ, Malmberg AB, Basbaum AI. 2001. PKCgamma contributes to a subset of the NMDA-dependent spinal circuits that underlie injury-induced persistent pain. J Neurosci 21(14):5321-7.

Matsubara A, Laake JH, Davanger S, Usami S, Ottersen OP. 1996. Organization of AMPA receptor subunits at a glutamate synapse: a quantitative immunogold analysis of hair cell synapses in the rat organ of Corti. J Neurosci 16(14):4457-67.

Maxwell DJ, Réthelyi M. 1987. Ultrastructure and synaptic connections of cutaneous afferent fibres in the spinal cord. Trends Neurosci 10(3):117-23.

Miletic V, Bowen KK, Miletic G. 2000. Loose ligation of the rat sciatic nerve is accompanied by changes in the subcellular content of protein kinase C beta II and gamma in the spinal dorsal horn. Neurosci Lett 288(3):199-202.

Miraucourt LS, Dallel R, Voisin DL. 2007. Glycine inhibitory dysfunction turns touch into pain through PKCgamma interneurons. PLoS One 2(11):e1116.

Miraucourt LS, Moisset X, Dallel R, Voisin DL. 2009. Glycine inhibitory dysfunction induces a selectively dynamic, morphine-resistant, and neurokinin 1 receptor- independent mechanical allodynia. J Neurosci 29(8):2519-27.

Miraucourt LS, Peirs C, Dallel R, Voisin DL. 2011. Glycine inhibitory dysfunction turns touch into pain through astrocyte-derived D-serine. Pain 152(6):1340-8.

Mori M, Kose A, Tsujino T, Tanaka C. 1990. Immunocytochemical localization of protein kinase C subspecies in the rat spinal cord: light and electron microscopic study. J Comp Neurol 299(2):167-77.

Mullen RJ, Buck CR, Smith AM. 1992. NeuN, a neuronal specific nuclear protein in vertebrates. Development 116(1):201-11.

Nakajima A, Tsuboi Y, Suzuki I, Honda K, Shinoda M, Kondo M, Matsuura S, Shibuta K, Yasuda M, Shimizu N, Iwata K. 2011. PKCgamma in Vc and C1/C2 is involved in trigeminal neuropathic pain. J Dent Res 90(6):777-81.

Nakamura K, Wu SX, Fujiyama F, Okamoto K, Hioki H, Kaneko T. 2004. Independent inputs by VG. Neuroreport 15(3):431-6.

Neumann S, Braz JM, Skinner K, Llewellyn-Smith IJ, Basbaum AI. 2008. Innocuous, not noxious, input activates PKCgamma interneurons of the spinal dorsal horn via myelinated afferent fibers. J Neurosci 28(32):7936-44.

Oancea E, Teruel MN, Quest AF, Meyer T. 1998. Green fluorescent protein (GFP)-tagged cysteine-rich domains from protein kinase C as fluorescent indicators for diacylglycerol signaling in living cells. J Cell Biol 140(3):485-98.

Olausson H, Wessberg J, Morrison I, McGlone F, Vallbo A. 2010. The neurophysiology of unmyelinated tactile afferents. Neurosci Biobehav Rev 34(2):185-91.

Oyasu M, Fujimiya M, Kashiwagi K, Ohmori S, Imaeda H, Saito N. 2008. Immunogold electron microscopic demonstration of distinct submembranous localization of the activated gammaPKC depending on the stimulation. J Histochem Cytochem. 56:253-65.

Paxinos G, Watson C. 1997. The rat brain in stereotaxic coordinates. New York: Academic Press.

Pfeiffer F, Simler R, Grenningloh G, Betz H. 1984. Monoclonal antibodies and peptide mapping reveal structural similarities between the subunits of the glycine receptor of rat spinal cord. Proc Natl Acad Sci U S A 81(22):7224-7.

Polgar E, Fowler JH, McGill MM, Todd AJ. 1999. The types of neuron which contain protein kinase C gamma in rat spinal cord. Brain Res 833(1):71-80.

Polgar E, Furuta T, Kaneko T, Todd A. 2006. Characterization of neurons that express preprotachykinin B in the dorsal horn of the rat spinal cord. Neuroscience 139(2):687-97.

Polgar E, Gray S, Riddell JS, Todd AJ. 2004. Lack of evidence for significant neuronal loss in laminae I-III of the spinal dorsal horn of the rat in the chronic constriction injury model. Pain 111(1-2):144-50.

Polgar E, Hughes DI, Riddell JS, Maxwell DJ, Puskar Z, Todd AJ. 2003. Selective loss of spinal GABAergic or glycinergic neurons is not necessary for development of thermal hyperalgesia in the chronic constriction injury model of neuropathic pain. Pain 104(1-2):229-39.

Polgar E, Sardella TC, Watanabe M, Todd AJ. 2011. Quantitative study of NPY-expressing GABAergic neurons and axons in rat spinal dorsal horn. J Comp Neurol 519(6):1007-23.

Ribeiro-da-Silva A, Coimbra A. 1982. Two types of synaptic glomeruli and their distribution in laminae I-III of the rat spinal cord. J Comp Neurol 209(2):176-86.

Sakai N, Sasaki K, Ikegaki N, Shirai Y, Ono Y, Saito N. 1997. Direct visualization of the translocation of the gamma-subspecies of protein kinase C in living cells using fusion proteins with green fluorescent protein. J Cell Biol 139(6):1465-76.

Sakai N, Tsubokawa H, Matsuzaki M, Kajimoto T, Takahashi E, Ren Y, Ohmori S, Shirai Y, Matsubayashi H, Chen J, Duman RS, Kasai H, Saito N. 2004. Propagation of gammaPKC translocation along the dendrites of Purkinje cell in gammaPKC-GFP transgenic mice. Genes Cells 9(10):945-57.

Schindelin J, Arganda-Carreras I, Frise E, Kaynig V, Longair M, Pietzsch T, Preibisch S, Rueden C, Saalfeld S, Schmid B, Tinevez JY, White DJ, Hartenstein V, Eliceiri K, Tomancak P, Cardona A. 2012. Fiji: an open-source platform for biological-image analysis. Nat Methods 9(7):676-82.

Schmid B, Schindelin J, Cardona A, Longair M, Heisenberg M. 2010. A high-level 3D visualization API for Java and ImageJ. BMC Bioinformatics 11:274.

Seal RP, Wang X, Guan Y, Raja SN, Woodbury CJ, Basbaum AI, Edwards RH. 2009. Injury-induced mechanical hypersensitivity requires C-low threshold mechanoreceptors. Nature 462(7273):651-5.

Strassman AM, Vos BP. 1993. Somatotopic and laminar organization of fos-like immunoreactivity in the medullary and upper cervical dorsal horn induced by noxious facial stimulation in the rat. J Comp Neurol 331(4):495-516.

Tardin C, Cognet L, Bats C, Lounis B, Choquet D. 2003. Direct imaging of lateral movements of AMPA receptors inside synapses. EMBO J 22(18):4656-65.

Todd AJ, Spike RC, Polgar E. 1998. A quantitative study of neurons which express neurokinin-1 or somatostatin sst2a receptor in rat spinal dorsal horn. Neuroscience 85(2):459-73.

Torsney C, MacDermott AB. 2006. Disinhibition opens the gate to pathological pain signaling in superficial neurokinin 1 receptor-expressing neurons in rat spinal cord. J Neurosci 26(6):1833-43.

Treede RD, Magerl W. 2000. Multiple mechanisms of secondary hyperalgesia. Prog Brain Res 129:331-41.

Vaccarino F, Guidotti A, Costa E. 1987. Ganglioside inhibition of glutamate-mediated protein kinase C translocation in primary cultures of cerebellar neurons. Proc. Natl. Acad. Sci. U.S.A. 84: 8707–11.

Waldvogel HJ, Baer K, Eady E, Allen KL, Gilbert RT, Mohler H, Rees MI, Nicholson LF, Faull RL. 2010. Differential localization of gamma-aminobutyric acid type A and glycine receptor subunits and gephyrin in the human pons, medulla oblongata and uppermost cervical segment of the spinal cord: an immunohistochemical study. J Comp Neurol 518(3):305-28.

Williams RW, Rakic P. 1988. Three-dimensional counting: an accurate and direct method to estimate numbers of cells in sectioned material. J Comp Neurol 278(3):344-52.

Wolf HK, Buslei R, Schmidt-Kastner R, Schmidt-Kastner PK, Pietsch T, Wiestler OD, Blumcke I. 1996. NeuN: a useful neuronal marker for diagnostic histopathology. J Histochem Cytochem 44(10):1167-71.

Woolf CJ. 2011. Central sensitization: implications for the diagnosis and treatment of pain. Pain 152(3 Suppl):S2-15.

Yevseyenkov VV, Das S, Lin D, Willard L, Davidson H, Sitaramayya A, Giblin FJ, Dang L, Takemoto DJ. 2009. Loss of protein kinase Cgamma in knockout mice and increased retinal sensitivity to hyperbaric oxygen. Arch Ophthalmol 127(4):500-6.

Zeilhofer HU, Wildner H, Yevenes GE. 2012. Fast synaptic inhibition in spinal sensory processing and pain control. Physiol Rev 92(1):193-235.

Zerari F, Fischer J, Sagot MA, Frobert Y, Couraud JY, Conrath M. 1998. Substance P receptor immunodetection in the spinal cord: comparative use of direct anti-receptor antibody and anti-complementary peptide antibody. Brain Res Bull 46:263-268.

Zou W, Song Z, Guo Q, Liu C, Zhang Z, Zhang Y. 2011. Intrathecal lentiviral-mediated RNA interference targeting PKCgamma attenuates chronic constriction injury-induced neuropathic pain in rats. Hum Gene Ther 22:465-75.

FIGURE LEGENDS

Figure 1: Rat brain and spinal cord tissue preparation probed with anti-$GABA_A$ receptor β2/β3 (left), anti-Glycine receptor (middle), or without primary antibody (right). In the spinal cord, the two bands observed with the anti-$GABA_A$ receptor antibody correspond to the β3 (57kDa), and β2 (55kDa) subunits. Glycine receptors (48kDa) appear more abundant in the spinal cord than in the brain. No signal was detected in control experiments, after omitting the primary antibodies.

Figure 2: PKCγ immunostaining in MDH. **A**: Fluorescence images from transverse sections through the MDH immunolabelled to reveal PKCγ using antibody sc-211. Left and right hemisections are from the very same section which has been cut on the middle. The left hemisection was pre-incubated for 30 min with the peptide p-sc-211 (40 $ng.ml^{-1}$) against which the antibody has been raised. Only the right hemisection displays the characteristic lamina II_i PKCγ immunostaining. Scale bar = 500 µm. **B-D**: Fluorescent images from transverse sections through the MDH lamina II_i immunolabelled to reveal PKCγ using the polyclonal antibody sc-211 (B) and monoclonal antibody P8083 (C). As seen on the merged image (D), PKCγ immunoreactive cells are immunolabelled by the two antobodies. Scale bar = 20 µm.

Figure 3. Schematic representation of the 300 x 400 µm cell counting window (pointed by arrow). Its median axe is positioned perpendicular to the MDH border (longest dotted line) and its dorsolateral end at the border between the white and grey matter. The center of this window (black dot) is set on the diagonal of a rectangle enclosing the whole MDH (black square). Scale bar = 500 µm.

Figure 4: Rostro-caudal distribution of PKCγ imunoreactivity whithin trigeminal MDH. **A-E**: PKCγ imunoreactivity in transverse sections at various levels (800 µm intervals) of the MDH, from its rostral (B: 0 µm; obex apperture) to its caudal end (E: -2400 µm). A transverse section at +400 µm, where the MDH and Sp5I overlap with each other, is displayed in addition (A). On the right are the corresponding schematic drawings of laminar organization. It is clear that PKCγ immunoreactivity occupies mainly the inner part of lamina II (lamina II_i). Thick and dense at the rostral end of MDH (-2400 µm), the lamina II_i band of PKCγ imunoreactivity becomes thinner (-1600 and -800 µm) and scattered (0 µm) when moving rostrally. It has diseapeared at +400 µm where the MDH and Sp5I are overlapping and the laminar organization is lost. Scale bars = 500 µm. I, lamina I. II, lamina II. III, lamina III. IV, lamina IV. V, lamina V. MDH, medullary dorsal horn. Sp5I, spinal trigeminal nucleus interpolaris.

Figure 5. Laminar distribution of NeuN and PKCγ immunoreactive cells within lamina I-IV of MDH. **A-C:** Confocal images showing NeuN (A), PKCγ (B) and merged NeuN and PKCγ (C) immunoreactivities in laminae I, II_o, II_i and III-IV. Border between layers are shown with dotted lines. Scale bar = 50 µm. **D:** Proportion of PKCγ immunoreactive cells in laminae I-IV. More than half of the total number of PKCγ immunoreactive cells are found in lamina II_i. **E:** Bar histogram of the relative number (mean + SEM) of NeuN/PKCγ immunoreactive neurons to the total number of NeuN immunoreactive neurons within each laminae I-IV. In lamina II_i, PKCγ immunoreactive cells represent about 1/3 of total neurons. Data are shown as mean ± SEM (n = 4).

Figure 6. Synaptic inputs to PKCγ immunoreactive interneurons. **A, B:** Axodendritic asymetric (A) and axosomatic symetric (B) synapses on a PKCγ immunoreactive cell (DAB

reaction). Arrows point to active zones. Scale bars = 500 nm. Pre, presynaptic. Post, postsynaptic. N, nucleus.

Figure 7. Primary afferent inputs to PKCγ immunoreactive interneurons. **A-C**: VGLUT3-immunostaining in the MDH. Light microscopic image through a transverse section of the MDH immunostained to reveal VGLUT3 (C) and the corresponding Neurolucida reconstruction (D). Dashed lines represent lamina I-II_o, II_o-II_i and II_i-III borders. Fibers coming from the Lissauer tract project ventrali through the most superficial layers and form a dense plexus within the inner part of the lamina II. Scale bars = 20 μm. **C**: Bar histogram of the normalized VGLUT3 immureactivity area to the total area of each lamina (I-III) (mean + SEM; n = 5). D: Electron microscopic image of an asymetric synapse between a primary afferent and a PKCγ immunoreactive interneuron (gold particles) in a type II glomerulus. Arrowscross asymetric synapses between the presynaptic terminal and postsynaptic dendrites (stars). Scale bar = 500 nm. Pre, presynaptic. Post, postsynaptic.

Figure 8. $GABA_A$ergic inputs to PKCγ immunoreactive interneurons. **A**: Colocalization of $GABA_A$ receptor immunoreactivity (gold particles) in a PKCγ immunoreactive interneuron (DAB reaction). Inset: higher magnification of the box. Scale bar = 1 μm. **B-D**: Bar histograms (mean + SEM) of the distribution of gold particles signaling $GABA_A$ receptor immunoreactivity to plasma membranes in PKCγ immunoreactive somatic (B, C) and dendritic (D) profiles. Distances are between the midpoint of each gold particle and the centre line of the associated plasma membrane. Extra- and intracellular positions are displayed together. Measurements were grouped in 200 nm (B) and 50 nm wide bins (C, D). Histogram in C is the same as in B but for the first 400 nm from somatic membranes. **E**: Areal density (number of particles. μm^{-2}) of gold particles signaling $GABA_A$ receptor immunoreactivity in

PKCγ immunoreactive somatic (left) and dendritic (right) profiles. Data are shown as both individual values (filled squares) and mean ± SEM (horizontal lines) (soma, n = 7; dendrites, n = 20).

Figure 9. Glycinergic inputs to PKCγ immunoreactive interneurons. **A**: Colocalization of glycine receptor immunoreactivity (gold particles) in a PKCγ immunoreactive interneuron (DAB reaction). Inset: higher magnification of the box. Scale bar = 2 µm. **B-D**: Bar histograms (mean + SEM) of the distribution of gold particles signaling glycine receptor immunoreactivity to plasma membranes in PKCγ immunoreactive somatic (B, C) and dendritic (D) profiles. Distances are between the midpoint of each gold particle and the centre line of the associated plasma membrane. Extra- and intracellular positions are displayed together. Measurements were grouped in 200 nm (B) and 50 nm wide bins (C, D). Histogram in C is the same as in B but for the first 400 nm from somatic membranes. **E**: Areal density (number of particles. μm^{-2}) of gold particles signaling glycine receptor immunoreactivity in PKCγ immunoreactive somatic (left) and dendritic (right) profiles. Data are shown as both individual values (filled squares) and mean ± SEM (horizontal lines) (soma, n = 7; dendrites, n = 20).

Figure 10. Subcellular localization of PKCγ immunoreactivity at the electron microscopic level. **A, B:** PKCγ immunoreactivity (DAB reaction) in a fusiform (A) and egg-shaped (B) PKCγ immunoreactive interneurons. Scale bars = 2 µm. **C.** Gold particles signaling PKCγ immunoreactivity in dendrites. Scale bars = 200 nm. Both techniques suggest that PKCγ immunoreactivity is predominantly located to plasma membranes (white arrows in A, B). **D.** Bar histogram (mean + SEM) of the distribution of gold particles signaling PKCγ immunoreactivity to plasma membranes. Distances are between the midpoint of each gold

particle and the centre line of the associated plasma membrane. Measurements were grouped in 10 nm wide bins. **E**: Example of clustered gold particles signaling PKCγ immunoreactivity on plasma membranes close to, but not on, synaptic densities. **F**: Bar histogram (mean + SEM) of the distribution of gold particles signaling PKCγ immunoreactivity to synaptic clefts. Distances are between the midpoint of each gold particle and the middle of the synaptic density. Measurements were grouped in 50 nm wide bins. PKCγ immunoreactivity was very rarely encountered in active zones but frequently formed clusters in the perisynaptic space. Extra- and intracellular positions are displayed together. . Arrows in C and E show putative endosomes, frequently located close to asymetric synapses. N, nucleus. C, centrosome.

Figure 11. Subcellular localization of PKCγ immunoreactivity in MDH lamina II_i interneurons and cerebellar Purkinje cells. **A, C:** Light microscopic image from a transverse section through MDH (A) and a coronal section through the cerebellar cortex (C) immunostained for PKCγ. Insets show higher magnifications of the respective selected neurons. Arrows point to nuclei, double arrows to plasma membranes and arrowheads to the cytoplasm. Scale bars = 20 μm. **B, D, F, G:** Confocal images of PKCγ immunoreactivity (B, D) and PKCγ gray levels (F, G) of a MDH lamina II_i interneuron (B, F) and cerebellar Purkinje cell (D, G). Gray values in F and G have been measured along the black lines in B and C, respectively. Vertical lines in B, D indicate changes in cellular compartments: plasma membrane to cytoplasm (full lines), cytopalsm to presumably nucleus (dotted lines). Changes in cell compartments in F, G are indicated with dotted lines. Scale bars in B, D = 10 μm. **E:** Bar histogram of the relative subcellular localization (plasma membrane: filled bars; perykarion: empty bars) of PKCγ immunoreactivity in MDH lamina II_i interneurons and Purkinje cells. Data are shown as mean ± SEM (n = 10 per group). ***, $p<0.0001$. **, $p<0.001$. Mb, plasma membrane. Cyt, Cytoplasm

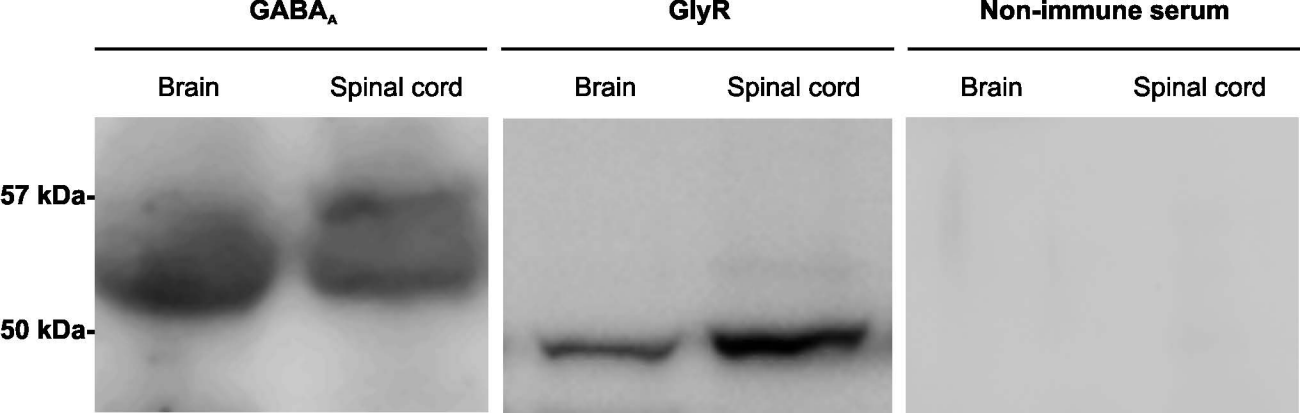
GABA$_A$
GlyR
Non-immune serum
Brain
Spinal cord
Brain
Spinal cord
Brain
Spinal cord
57 kDa-
50 kDa-

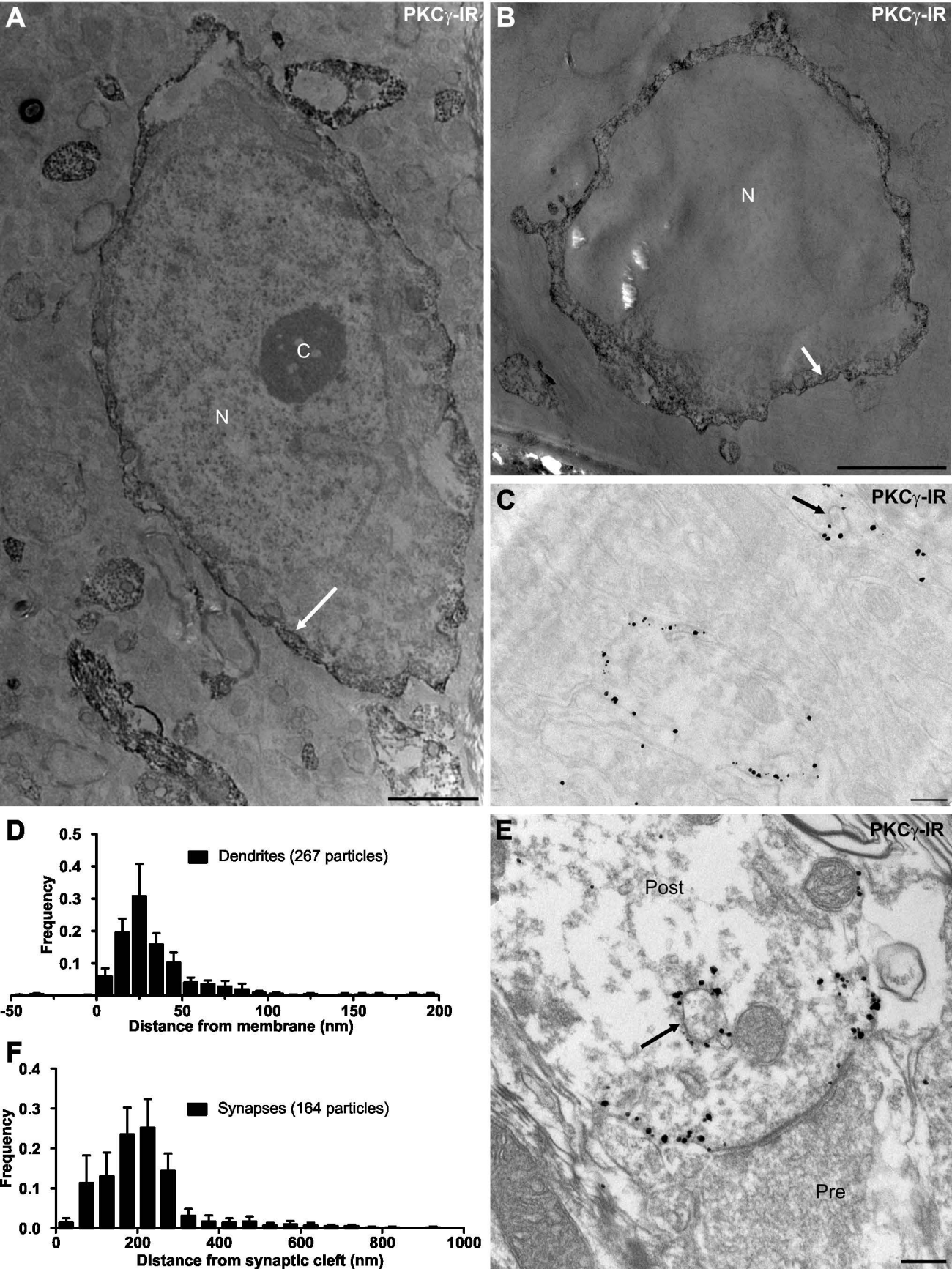
A
PKCγ-IR
C
N
B
PKCγ-IR
N
C
PKCγ-IR
D
Dendrites (267 particles)
Frequency
0.5
0.4
0.3
0.2
0.1
-50
0
50
100
150
200
Distance from membrane (nm)
E
PKCγ-IR
Post
Pre
F
Synapses (164 particles)
Frequency
0.4
0.3
0.2
0.1
0.0
0
200
400
600
800
1000
Distance from synaptic cleft (nm)

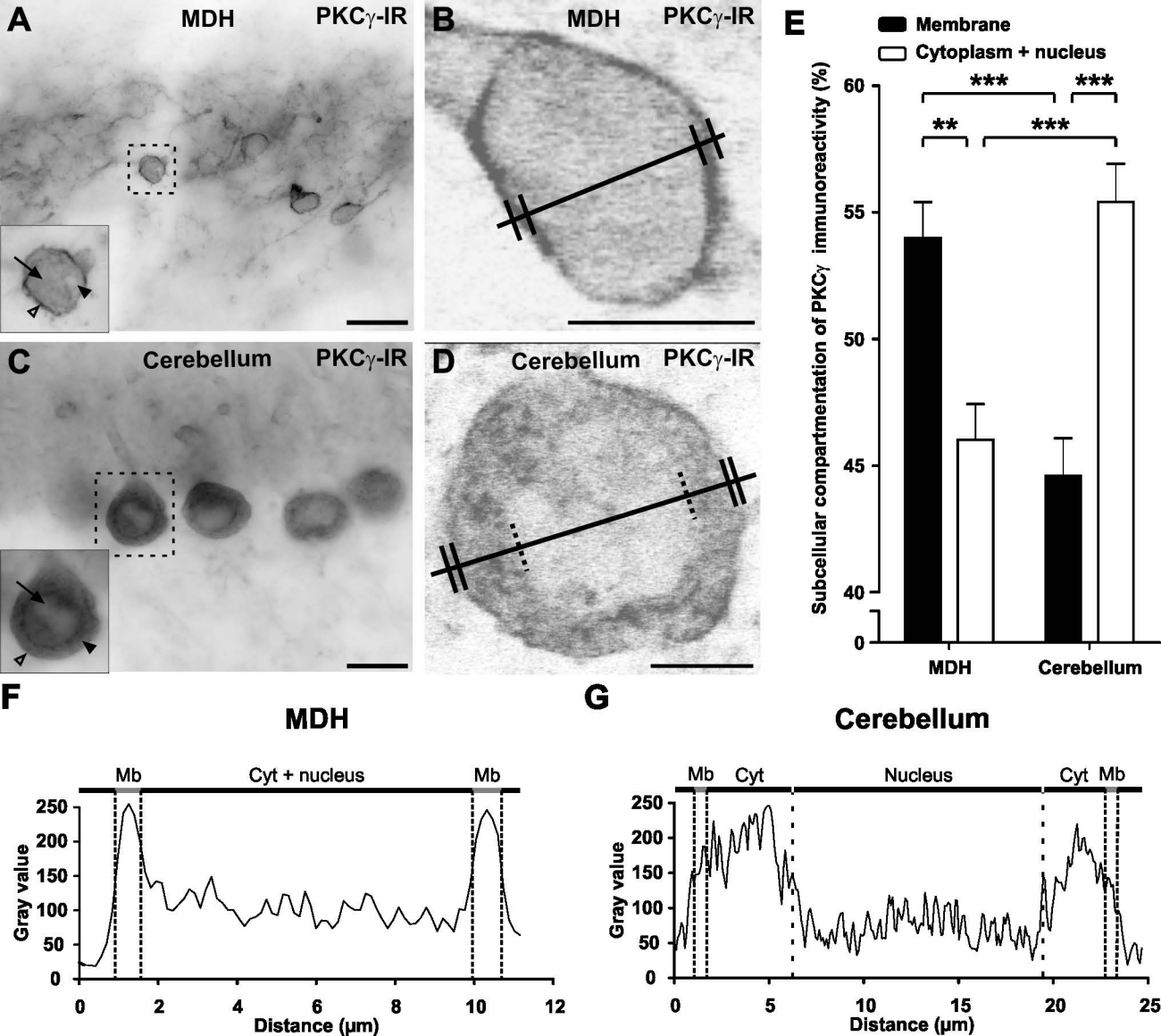
A
MDH
PKCγ-IR
B
MDH
PKCγ-IR
C
Cerebellum
PKCγ-IR
D
Cerebellum
PKCγ-IR
E
Membrane
Cytoplasm + nucleus
Subcellular compartmentation of PKCγ immunoreactivity (%)
60
55
50
45
40
0
***
***
**
***
MDH
Cerebellum
F
MDH
Mb
Cyt + nucleus
Mb
Gray value
250
200
150
100
50
0
0
2
4
6
8
10
12
Distance (μm)
G
Cerebellum
Mb
Cyt
Nucleus
Cyt
Mb
Gray value
250
200
150
100
50
0
0
5
10
15
20
25
Distance (μm)

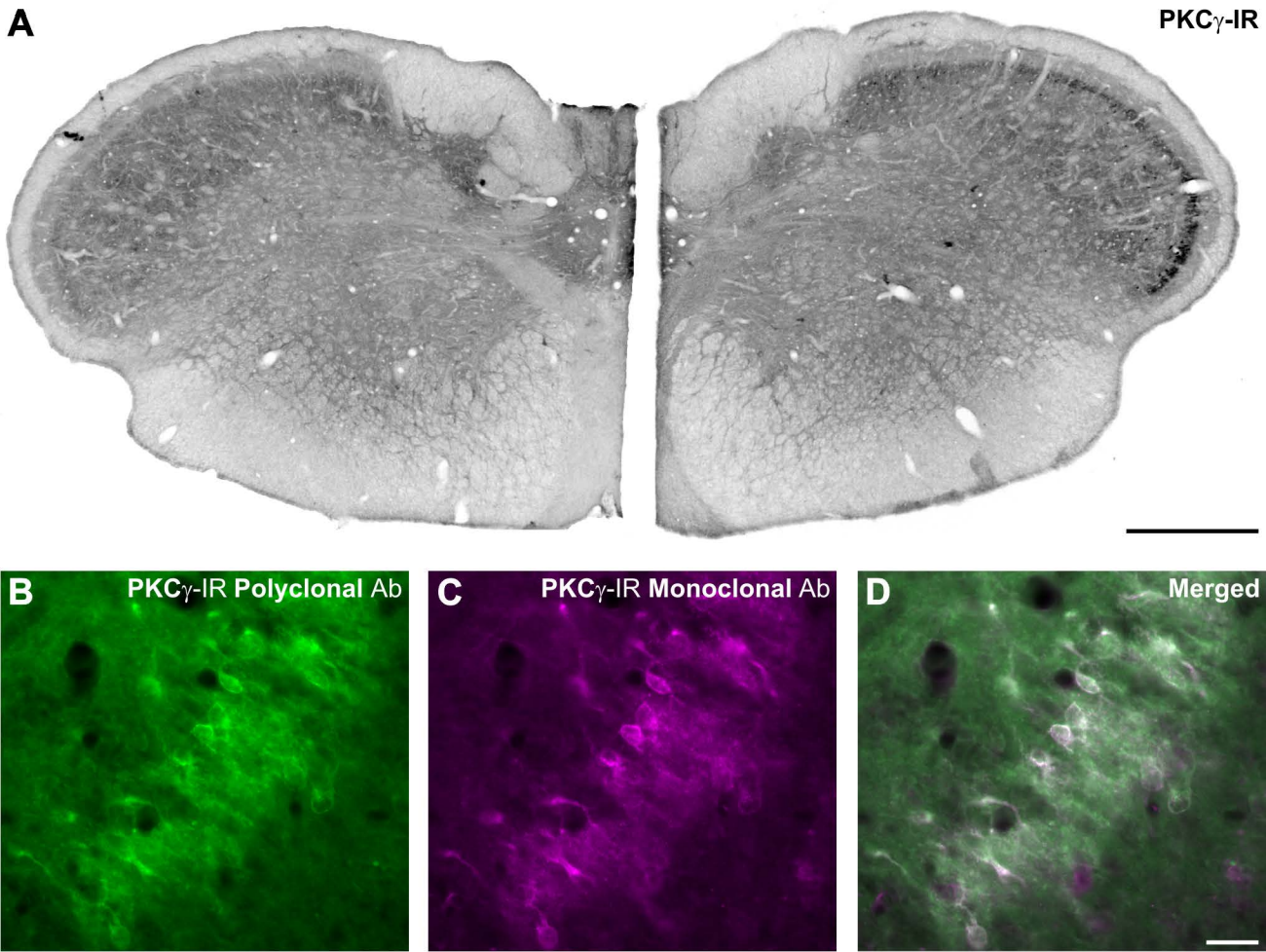
A
PKCγ-IR
B
PKCγ-IR Polyclonal Ab
C
PKCγ-IR Monoclonal Ab
D
Merged

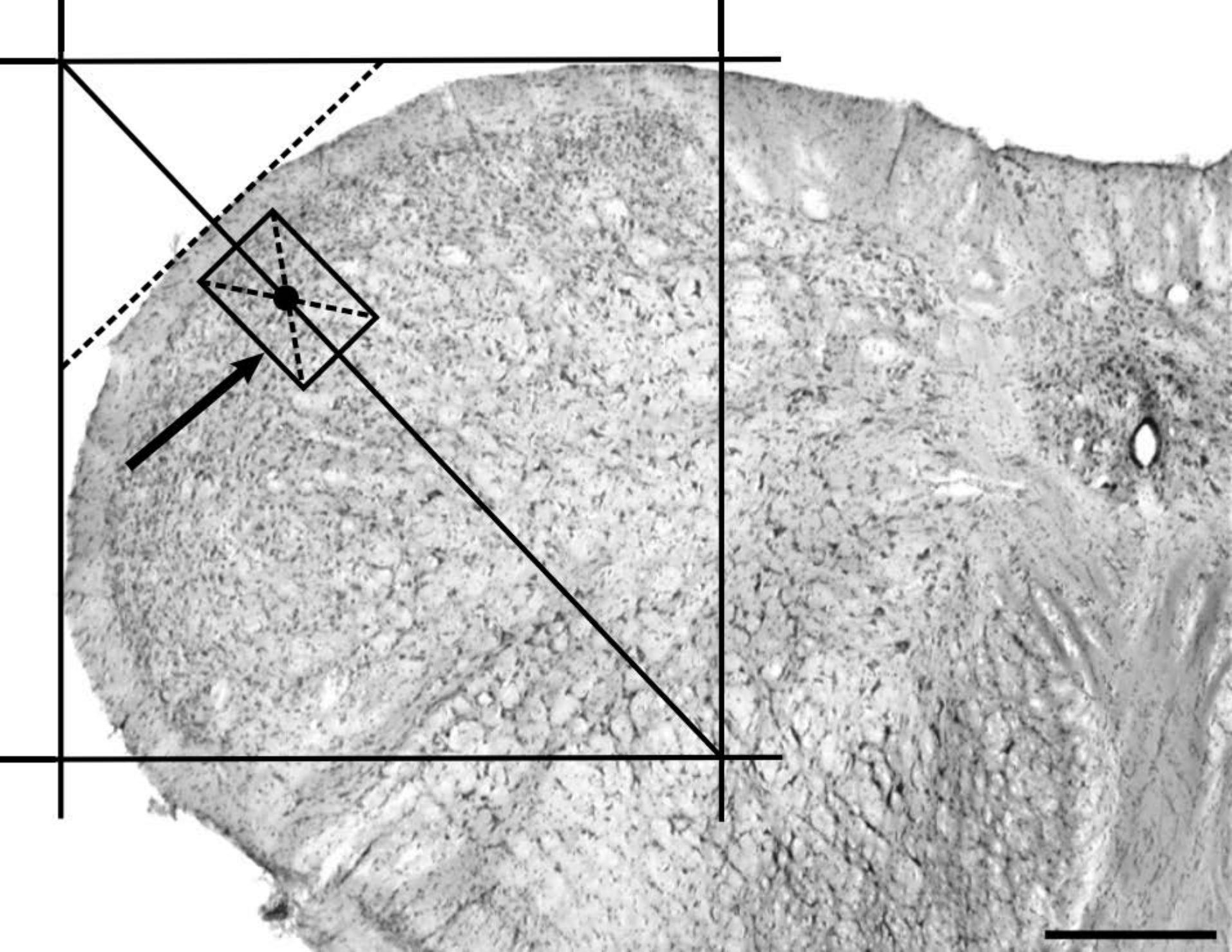

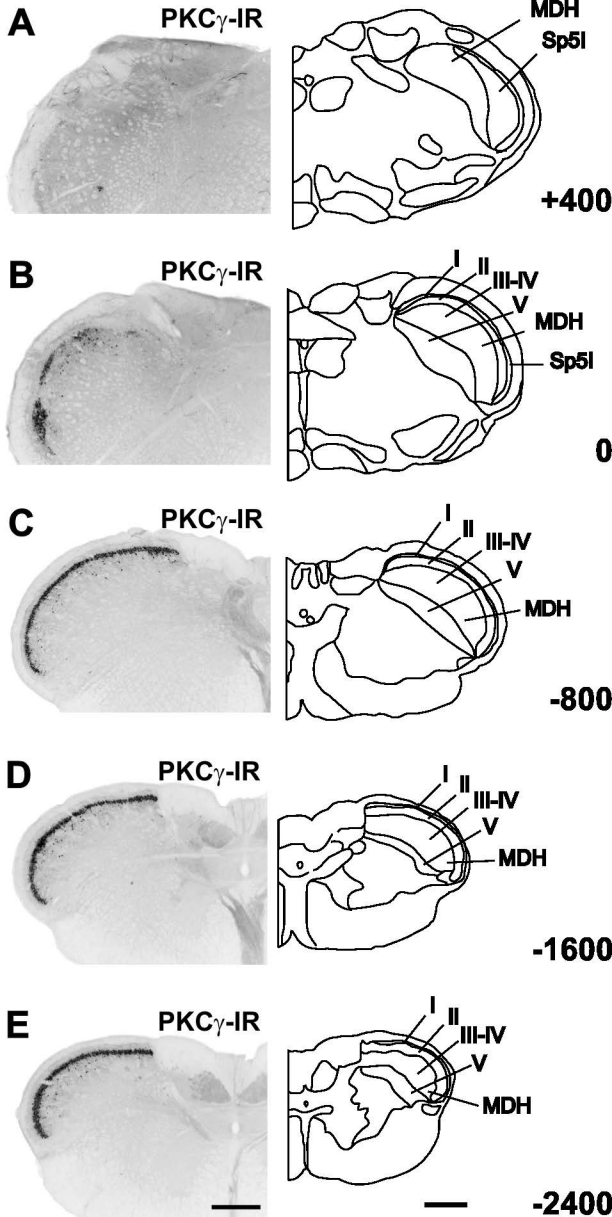
A
PKCγ-IR
MDH
Sp5I
+400
B
PKCγ-IR
I
II
III-IV
V
MDH
Sp5I
0
C
PKCγ-IR
I
II
III-IV
V
MDH
-800
D
PKCγ-IR
I
II
III-IV
V
MDH
-1600
E
PKCγ-IR
I
II
III-IV
V
MDH
-2400

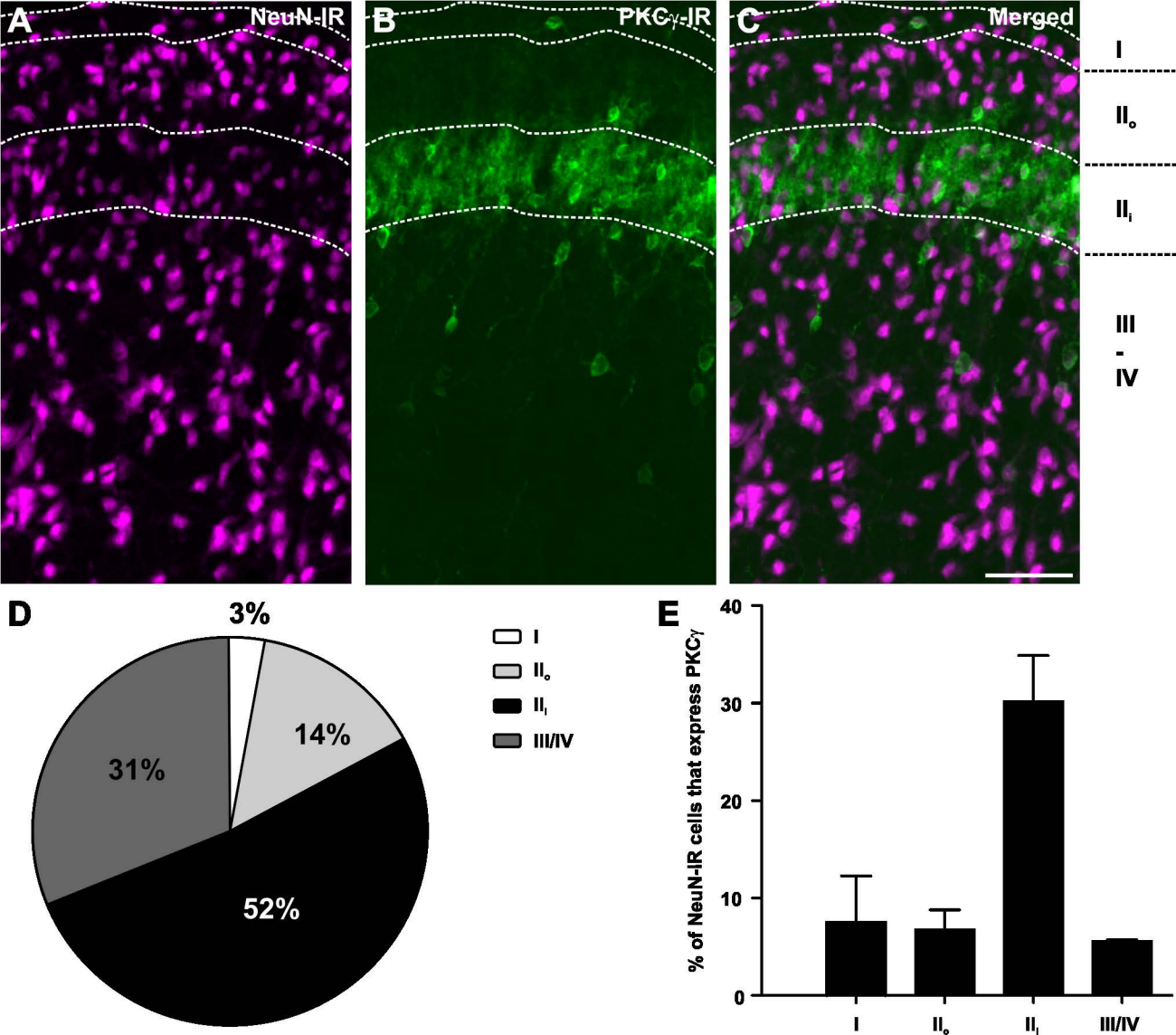
A
NeuN-IR
B
PKCγ-IR
C
Merged
I
IIo
IIi
III
-
IV
D
3%
14%
31%
52%
I
IIo
IIi
III/IV
E
% of NeuN-IR cells that express PKCγ
40
30
20
10
0
I
IIo
IIi
III/IV

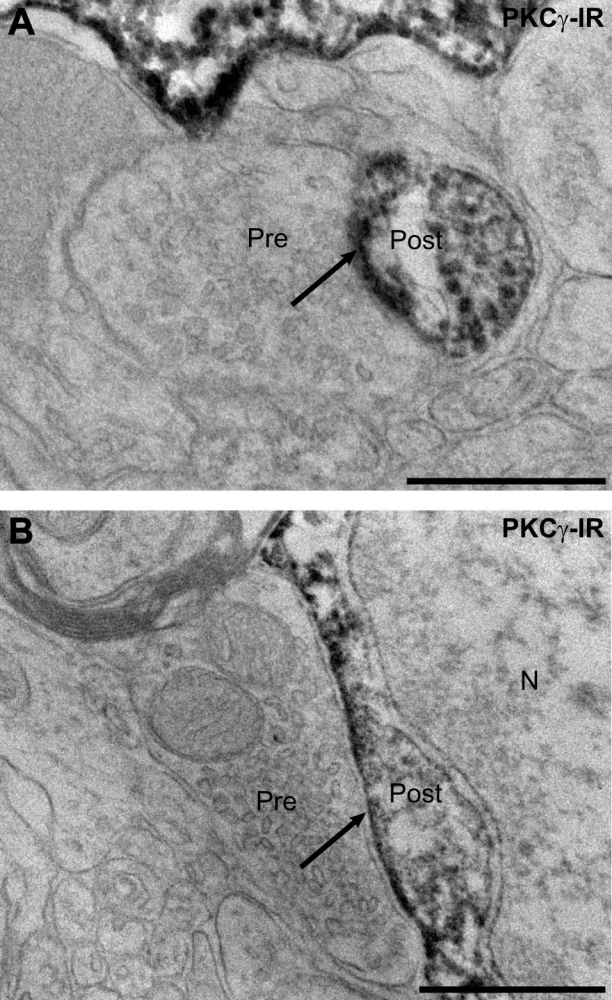
A
PKCγ-IR
Pre
Post
B
PKCγ-IR
N
Pre
Post

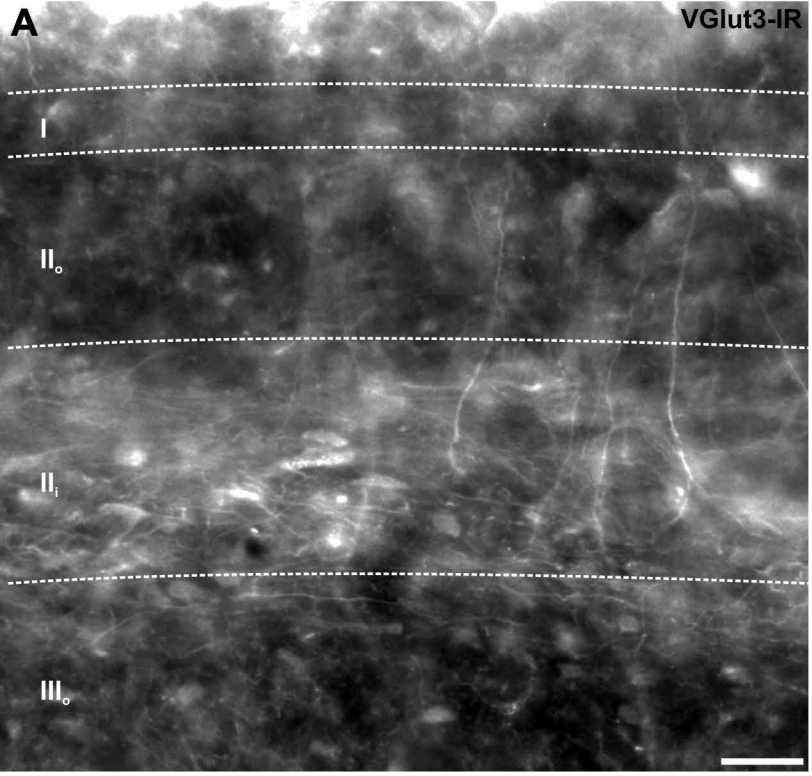
A
VGlut3-IR
I
II$_o$
II$_i$
III$_o$

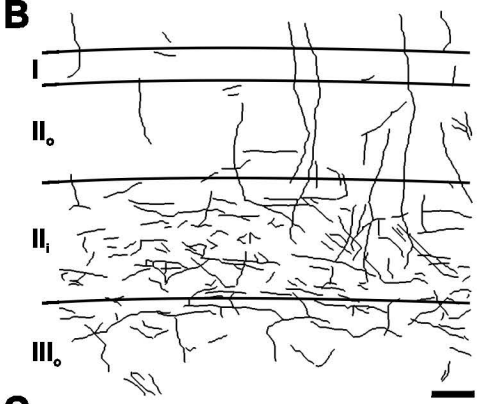
B
I
II$_o$
II$_i$
III$_o$

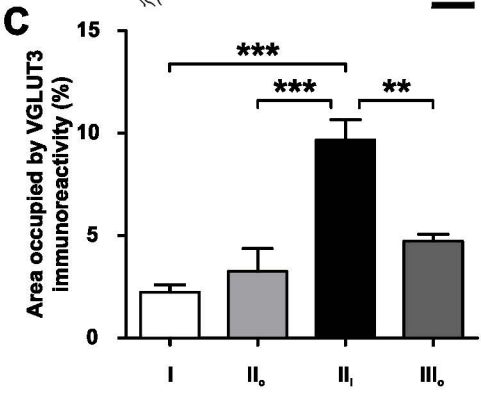
C
Area occupied by VGLUT3 immunoreactivity (%)
15
10
5
0
***
***
**
I
II$_o$
II$_i$
III$_o$

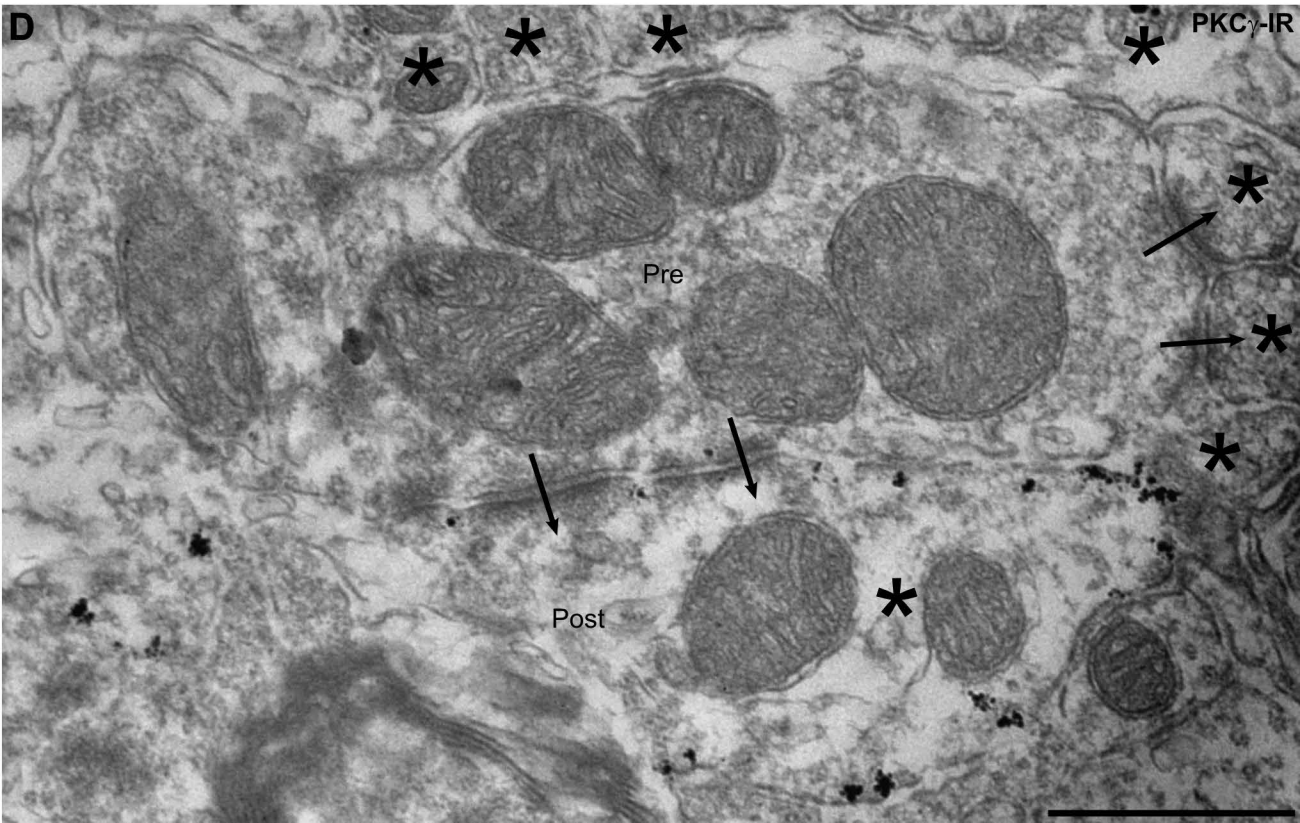
D
PKCγ-IR
Pre
Post

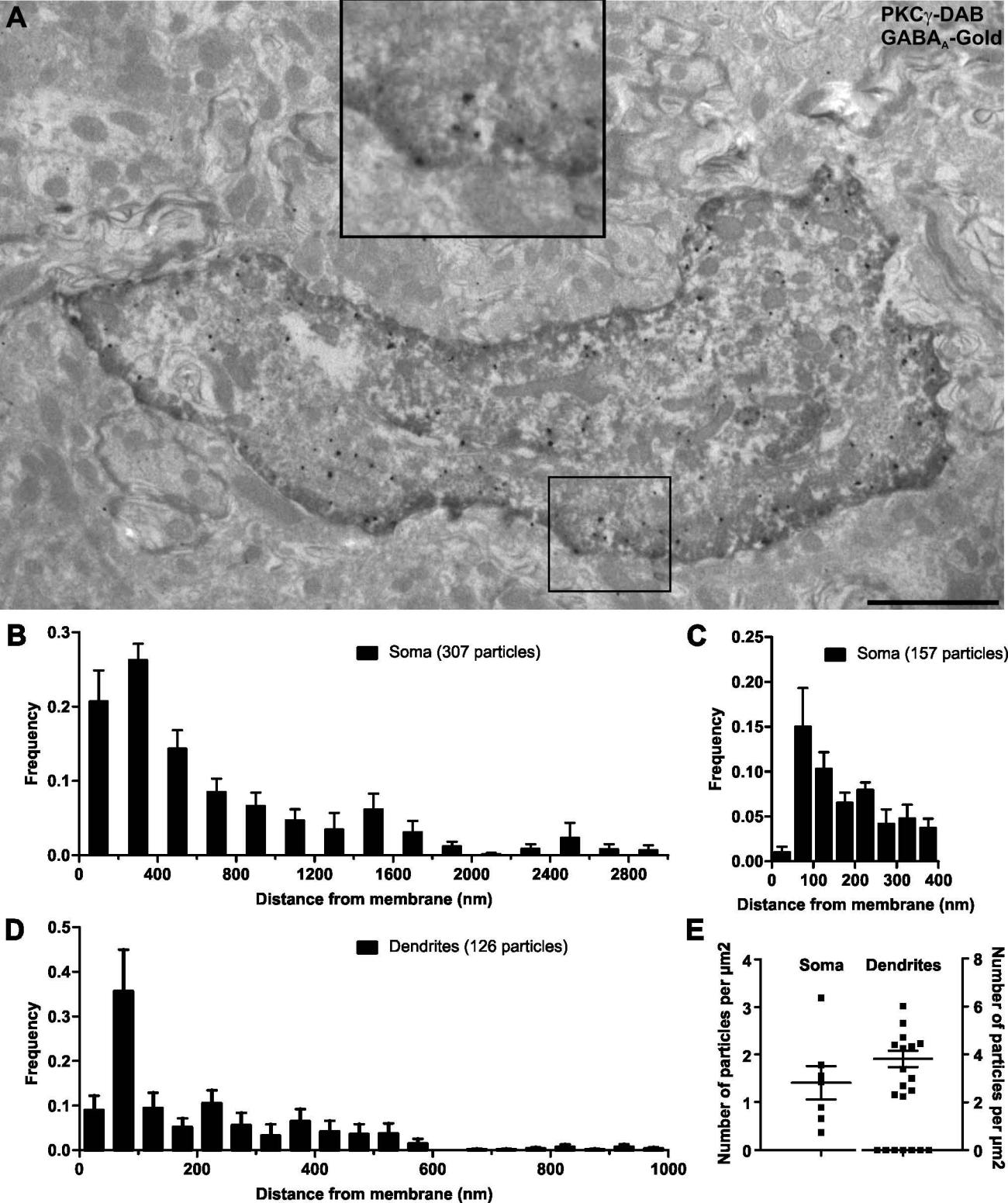
A
PKCγ-DAB
GABA$_A$-Gold
B
Soma (307 particles)
Frequency
0.3
0.2
0.1
0.0
0
400
800
1200
1600
2000
2400
2800
Distance from membrane (nm)
C
Soma (157 particles)
Frequency
0.25
0.20
0.15
0.10
0.05
0.00
0
100
200
300
400
Distance from membrane (nm)
D
Dendrites (126 particles)
Frequency
0.5
0.4
0.3
0.2
0.1
0.0
0
200
400
600
800
1000
Distance from membrane (nm)
E
Soma
Dendrites
Number of particles per µm2
4
3
2
1
0
8
6
4
2
0
Number of particles per µm2

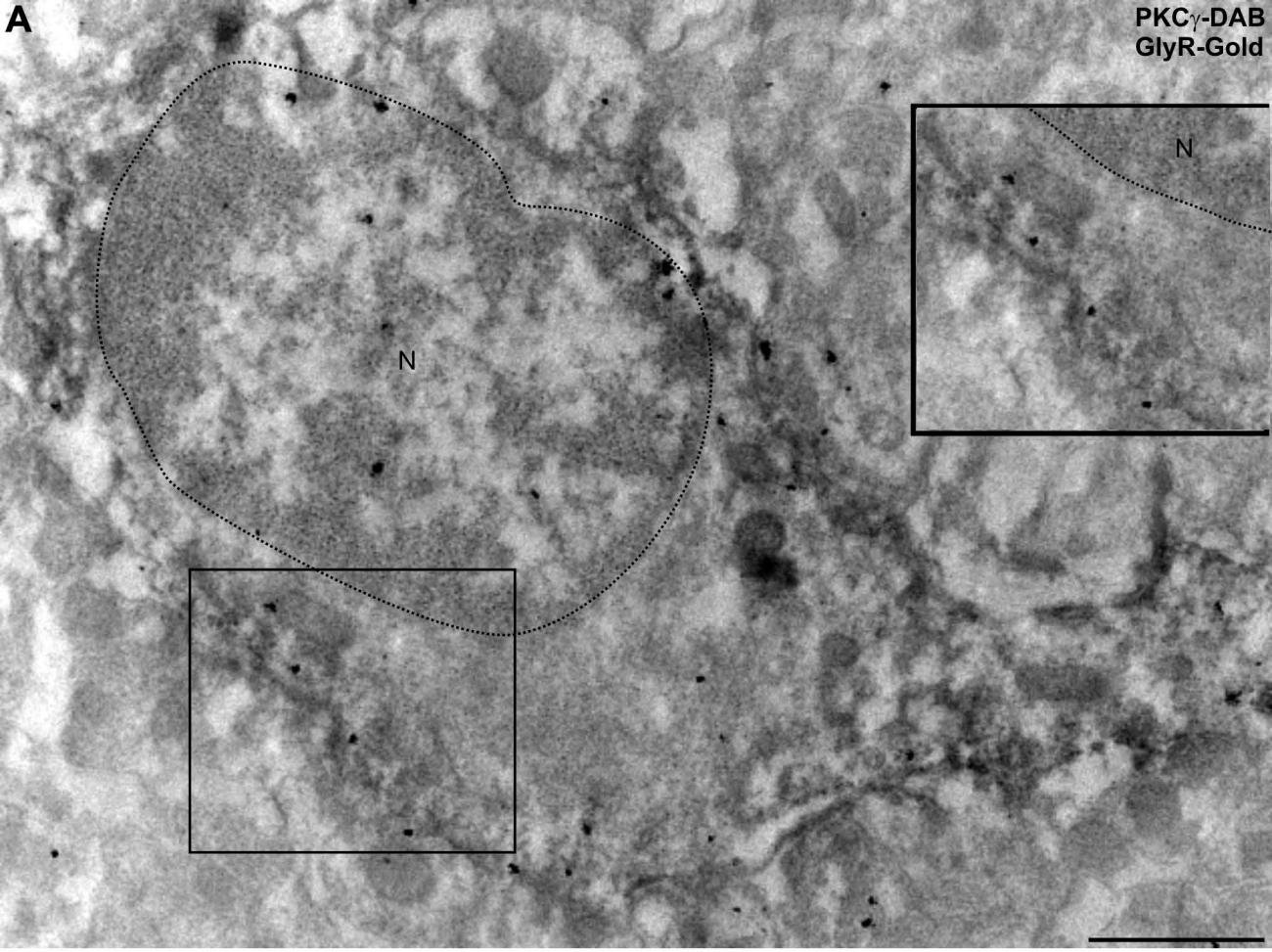
A
PKCγ-DAB
GlyR-Gold
N
N

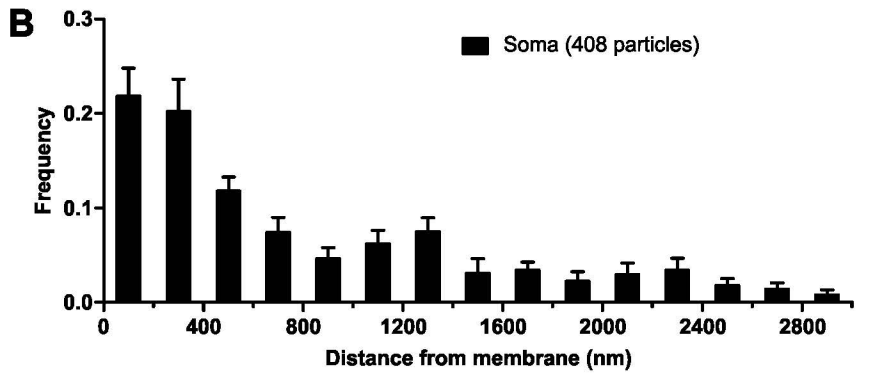
B
Soma (408 particles)
Frequency
0.0
0.1
0.2
0.3
0
400
800
1200
1600
2000
2400
2800
Distance from membrane (nm)

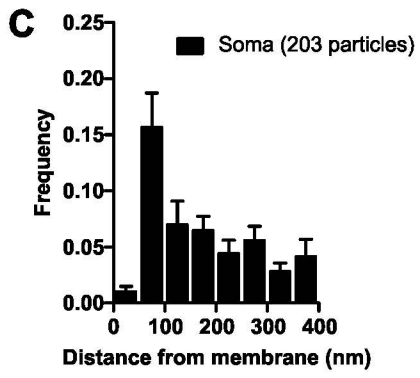
C
Soma (203 particles)
Frequency
0.00
0.05
0.10
0.15
0.20
0.25
0
100
200
300
400
Distance from membrane (nm)

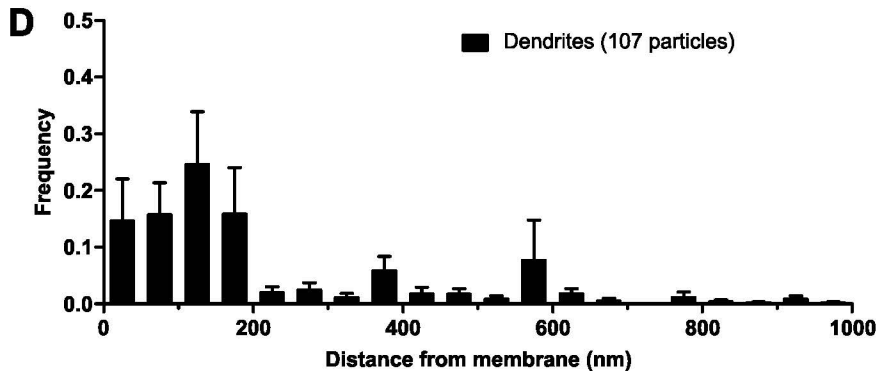
D
Dendrites (107 particles)
Frequency
0.0
0.1
0.2
0.3
0.4
0.5
0
200
400
600
800
1000
Distance from membrane (nm)

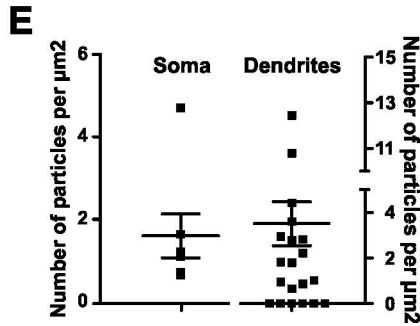
E
Soma
Dendrites
Number of particles per µm2
0
2
4
6
Number of particles per µm2
0
2
4
11
13
15